A CALORIMETRIC STUDY OF LIGHT HYDROCARBON ADSORPTION ON METAL-ORGANIC FRAMEWORKS

BY

TAYLOR BARRETT

A Thesis Submitted to the Graduate Faculty of

WAKE FOREST UNIVERSITY GRADUATE SCHOOL OF ARTS AND SCIENCES

in Partial Fulfillment of the Requirements

for the Degree of

MASTER OF SCIENCE

Chemistry

May 2019

Winston Salem, North Carolina

Approved By:

Michael D. Gross, PhD., Advisor

Ulrich Bierbach, PhD, Chair

Amanda C. Jones, PhD.

Acknowledgements

I would like to first thank my graduate committee; Dr. Amanda Jones, Dr. Ulrich Bierbach and Dr. Michael Gross, without whom this thesis would not exist. I also want to thank them for their guidance, advice and support throughout the program, which has made me a better scientist. I would like to thank the faculty and staff of the Department of Chemistry and Department of Engineering for sharing their mentorship and scholarship with me. I would also like to thank Dr. Cynthia Day for fostering my love of crystallography, for sharing the same passion for knowledge as me, and for her tireless work in my name. Most of the technical information in this thesis would not exist without Dr. Day's input, and the knowledge she gave me helped shape my future work.

I would like to thank fellow graduate students Jennifer Roberts and Trey Williams for their technical support and advice. I would also like to thank my fellow lab-mate Sixbert Muhoza for sharing information and equipment.

I would like to personally and professionally thank Jennifer Roberts for all her work and time she dedicated prior to me taking this project. Without Jennifer, these measurements would have been brutal and taken longer than they did. Jennifer not only gave her time to this research but also guided me throughout graduate school. Jen's mentorship, kindness and upbeat attitude kept me sane and grounded, and I continue to look to her as role model in all my endeavors.

I would like to thank Wake Forest University and the National Science Foundation for supporting me financially.

I would like to thank my research advisor of four years, Dr. Michael Gross, whose chaotic and creative approach to research always kept me learning. Dr. Gross fostered my love of chemistry and allowed me to explore, make mistakes and grow throughout these projects. His understanding and patience as I struggled through classes, calorimetry, and figuring out the kind of scientist I am means the world.

Finally, I would like to thank my family for their love and judgement. I want to thank my best friend Megan Dupriest, for her companionship, support and computer know-how. And I would like to thank my parents, whose constant presence in my life and pride in my accomplishments made this all worthwhile.

Table of Contents

Figures and Tables

List of Abbreviations

BZA	Benzoic acid
DMF	Dimethyl formamide
EtOH	Ethanol; also known as ethyl alcohol
GC-MS	Gas Chromatography-Mass Spectrometry
HAc	Acetic acid
HCl	Hydrochloric acid
H_4DOBDC	2,5-dihydroxyterephthalic acid, also known as H_4DOT
HKUST-1	Copper benzene-1,3,5-tricarboxylate MOF
MOF	Metal Organic Framework
MOF-5	Zirconium 1,4-benzodicarboxylate MOF
MOF-74	M2-dioxidoterephthalate MOF (M= Fe, Ni, Co etc.)
PXRD	Powder x-ray diffraction
SCXRD	Single crystal x-ray diffraction analysis
TPA	Benzene 1,4-dicarboxylic acid; also known as terephthalic acid
TPA-NH_2	2-aminoterephthalic acid
TPA-NO_2	2-nitroterephthalic acid

TGA	Thermogravimetric analysis
UiO-66	Zirconium 1,4-dicarboxybenzene MOF

Abstract

The effect of metal-organic framework (MOF) structural modifications on C_2 hydrocarbon gas adsorption was studied. Two main MOF structures were modified and tested: UiO-66, which has two types of pores in the structure and can support various functional groups on the organic linker, and MOF-74, which can support a multi-metal cluster. The adsorption of C_2 hydrocarbons on UiO-66 and UiO-66 functionalized with $–NH_2$ and $–NO_2$ was investigated to assess the role of confinement and electrostatic potential on binding energies at 293 K. Measurements were also collected at 195 K to better resolve the binding energies of the different types of adsorption sites. Confinement effects at the adsorption site and electrostatic potential of the adsorbate both contribute to the strength of the interaction within the lattice. The adsorption behavior at low coverage suggests that an unexpected third type of binding site is present in the MOF, which was further explored by studying adsorption behavior of UiO-66 with induced missing linker defects. MOF-74 was synthesized with cobalt, nickel, copper and combinations of Cu-Co, Ni-Co, and Cu-Ni to assess the adsorption behavior of mixed-metal MOFs. In all cases, the mixed-metal MOF binding energies were either equal to or lower than the single metal MOF samples. Overall, the UiO-66 study provides new insights into the adsorption behavior of C_2 hydrocarbons and the types of UiO-66 binding sites. The MOF-74 data illustrates that mixed-metal MOFs can be synthesized based on phase requirements, and that the effect of mixed metal clusters on the binding energy depends on the adsorbate.

1. Introduction

Since their introduction to the scientific community in the 1990s, metal-organic frameworks (MOFs) have attracted significant interest from academia and industry alike.[1] Metal-organic frameworks are nanomaterials self-assembled by metal clusters and organic linkers, creating a long-range ordered crystalline porous structure. MOFs are essentially a synthetic zeolite.[1] While zeolites are inorganic and occur naturally, MOFs are synthetic hybrid inorganic-organic materials that give rise to thousands of unique structures, allowing for more control over the final shape and surface area of the material.[1] Omar Yaghi coined the term metal-organic framework in 1995; he later went on to publish one of two key MOF papers in 1999, reporting a compound that had a surface area many times larger than the most porous zeolite.[1] This finding is significant because zeolites are widely used for gas processing; larger surface areas have a higher concentration of gas processing active sites.

1.1 MOF Technology

The two main components of a MOF are an organic linker and metal clusters.[2] The clusters and linkers self-assemble, forming nanocrystals with high surface areas and a highly symmetrical lattice system.[1,2] The organic linkers are the defining difference between MOFs and zeolites. Zeolites are aluminosilicate minerals, leading to uncontrollable and unpredictable pore sizes throughout the material.[1] The organic linker in MOFs form struts between the metal sites, giving larger pores with a uniform distribution. A comparison is shown in Figures 1-1 and 1-2:

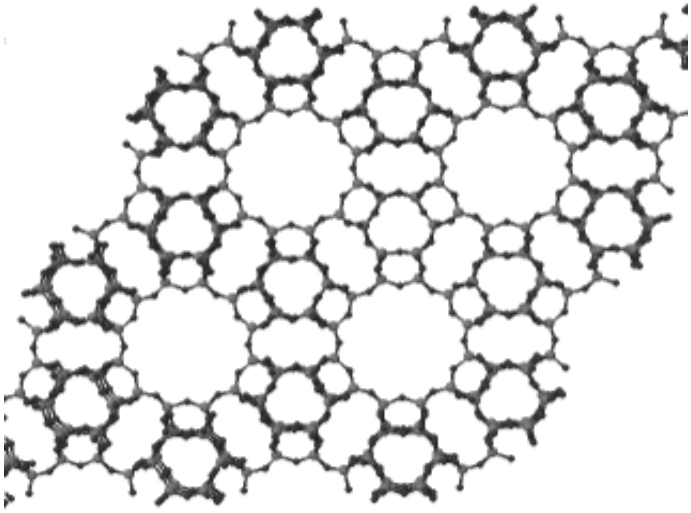

Figure 1-1: A line and ball graphic of MFI (ZSM-5) lattice structure. Zeolite is composed of SiO4 clusters linked by oxygen atoms.[3]

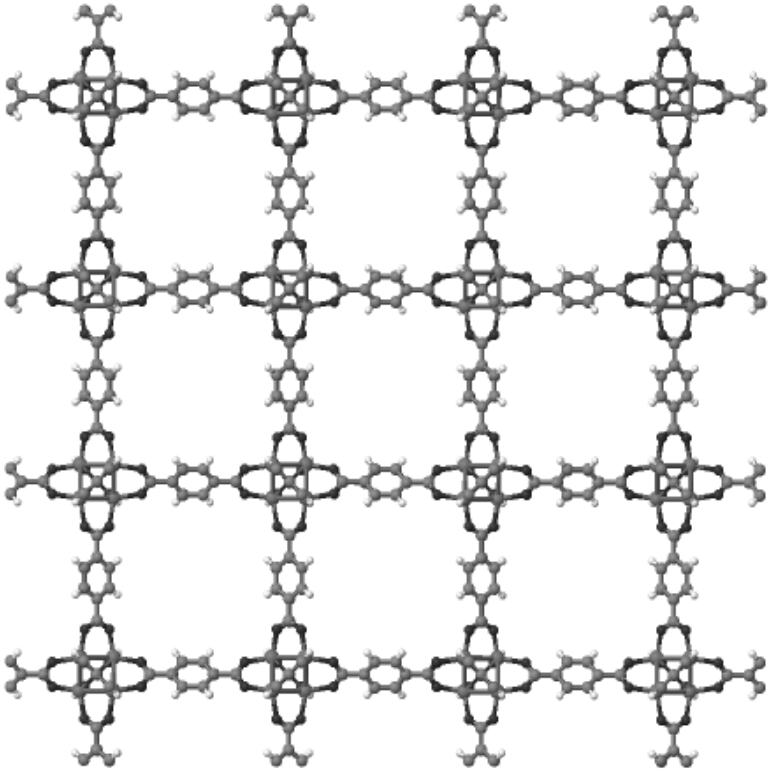

Figure 1-2: A line and ball graphic of MOF-5 lattice structure. MOF is composed of Zn_4O nodes and TPA linkers.[3]

Depending on the metal and linkers used, the pores can be any of a wide range of polygonal shapes. The simplest is MOF-5, which has a cubic structure, and one of the more complex ones, HKUST-1, has multiple pore shapes and sizes within the structure.[3] In addition to highly controllable physical properties, the chemical properties of MOFs can also be easily modified.[3, 4] For example, a wide range of functional groups can be attached to the basic organic linker building block.[4-7] The ease of modifying the physical and chemical properties of MOFs makes them an ideal class of materials for research.

The primary active sites of the MOF are the metal clusters; they often have a charge or polarizability that makes them ideal for short term Van der Waals interactions with other molecules, stabilizing those molecules within the pores.[4-6] Further, confinement effects within a MOF pore can also help stabilize molecules in the lattice. It turns out that gas molecule adsorption in MOFs is thermodynamically reversible, making MOFs ideal for applications in gas adsorption.[1-2,4-11]

For MOFs to be industrially relevant for gas adsorption applications, they must exhibit thermal stability and chemical stability in the presence of humidity.[4,8-11] The metal clusters play a critical role in both thermal and chemical stability. Highly coordinated metal clusters tend to be more stable.[4,5] For example, one of the most stable MOFs reported in the literature, UiO-66, has 12 organic linkers coordinated to every metal cluster.[5]

The self-assembly of the MOF happens on a lattice created by hydrogen bonding within the mother liquor. Organic solvent, mostly DMF or ethanol, disrupt the lattice to create small nanocrystals, while larger amounts of water create larger, misshapen particles.[12] Small particles are ideal because they have a larger surface area.[1] Prior to use, the open pores are filled with guest solvent trapped in the pores during formation.[2] This solvent must be removed prior to use. Removal is achieved by soaking the MOF solids in a low boiling point solvent to replace the mother liquor in the pores.[All] This solvent is then heated under vacuum; the liquid solvent is boiled and pulled from the pores, leaving them open for other molecules to fill.[All] At this point, the MOF must be kept under an inert

atmosphere to prevent atmospheric gases and water from filling those vacant binding sites prematurely.

1.2 MOF Usage and Limitations

The MOF structure is ideal for gas adsorption due to its open lattice and multiple binding sites.[1-2, 5-8] The sponge-like interior particularly makes it easy to add and remove components preferentially, and the stability of the metal sites makes the MOF reusable for multiple cycles.[13] The most important part of designing a MOF for adsorption of a specific gas is avoiding irreversible binding of the gas molecule to the binding site.[14] Once a molecule has adsorbed irreversibly, the gas molecule can never be desorbed and recovered.[14]

One form of industrial use for MOFs is in energy storage. A gas-based energy storage system is generally considered to be cheaper, more efficient, and "greener" than a coal or petroleum-based system.[15-18] Current technology uses steel compression tanks, which are heavy and dangerous, to store gases for use. Further, the tanks must be loaded under extreme pressure and stored under ambient conditions.[18] MOF technology offers the potential to trap and store gases for energy use under ambient conditions.[10,13-18] Hydrogen gas is one of the main targets for MOF advancement, though other high energy gases like hydrocarbons could also be processed this way.[19]

Another proposed usage of MOFs is as a replacement for cryogenic gas separations. Ethylene is one of the most produced chemicals in the petrochemical industry-170 million tons worldwide in 2016.[20] Production is very energy intensive and costly, due to the required olefin/paraffin separations.[21-23] The key factor is separating ethane, ethylene and acetylene; all similar in size and volatility. The current method requires both cryogenic distillations and catalytic separations, which are expensive in both costs and resources.[23] Adsorption-based separation is regarded as one of the most promising alternatives, and finding MOFs with suitable properties for this job has prompted interest in structure design and modification.[8,22,24]

The main issue with MOF systems is stability in atmospheric conditions and scaling to industrial targets. For a MOF to be viable in industrial settings, it must have a very high thermal stability and be stable in the presence of atmospheric water.[4-11,25-27] In most systems, water hydrolyzes bonds between the linker and metal cluster, leading to deterioration of the structure.[16] Considering the time and resources used to manufacture these compounds, constant replacement is not desirable. Further, MOFs that are stable under these conditions have more limited functionalization options, as the metal clusters that give water stability cannot be modified.[13] Considering the main drive for MOF research is the flexibility in almost any aspect of the structure, this is a glaring limitation. However, the organic linker can be modified with additional functional groups, which is a new topic of research.[6-7,25-26,28-30] The work represented in this thesis seeks to explore two ways of modifying MOFs for industrial use: varying the metal content of the clusters and functionalizing linkers.

1.3 Calorimetry and the Technique Used

Calorimetry is a technique that measures the heat released or absorbed by a material as in undergoes a reaction or physical change. Calorimeters measure changes in enthalpy (ΔH), or the heat energy present during a process.[30,31] Calorimeters are designed based on the material they are testing, the reaction being recorded, and the form of energy being measured. The main calorimetry technique used in MOF adsorption studies are isosteric heat measurements[31], but the work described in this thesis uses direct energy measurements.

Calorimetry is one method of testing and appraising MOF performance and functionality. The heat of adsorption, or energy released as gas is introduced to an active MOF, is used to assess the strength of interaction between an adsorbate and the adsorbent.[32] In most MOF research, the heat of adsorption is calculated by comparing isotherms collected at differing temperatures.[30,32] Isosteric measurements indirectly calculate the differential enthalpy of the MOF, rather than the direct energy released during the event.[31] This method has a significant limitation at low temperature. The isosteric calculation relies on the differences in pressure, but at low temperatures, the pressure changes very little resulting in inaccurate heat calculations.[32-35] Low-temperature measurements provide a great deal of insight into the adsorption behavior in MOFs because at higher temperatures,

the isosteric heats represent an average heat over all types of binding sites in the MOF.[32] MOFs oftentimes have multiple adsorption sites, and these sites have different strengths of adsorption. Low temperature adsorption measurements allow one to isolate the heat of adsorption for each type of binding site and the concentration of each type of binding site.[21] To isolate heats of adsorption and quantify the concentration of different types of adsorption sites, one must use adsorption calorimetry.[32] My thesis used a home-built Tian-Calvet adsorption calorimeter to make these measurements.

Tian-Calvet style calorimeters are specifically designed for adsorption studies; a schematic of the calorimeter is shown in Figure 1-3:

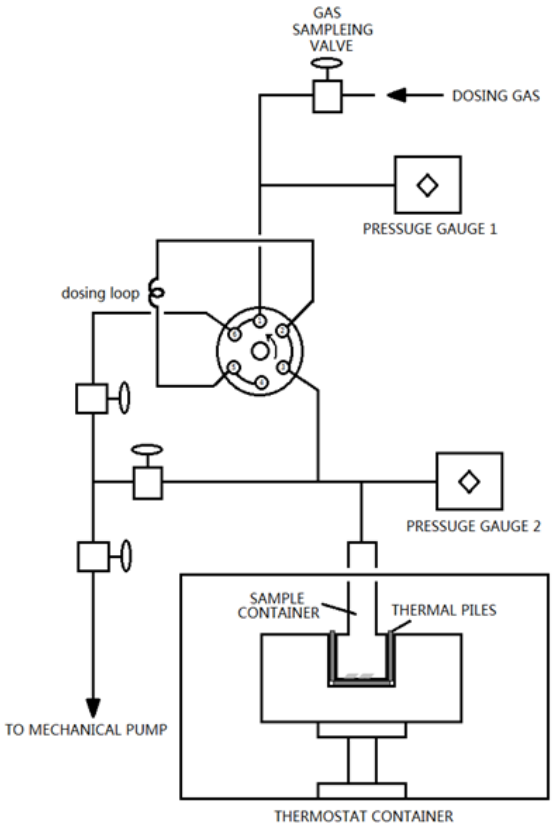

Figure 1-3: A schematic of the Tian-Calvet Adsorption calorimeter used for these projects. Original figure provided by the Gorte lab at the University of Pennsylvania

The critical feature of the calorimeter is that adsorbates can be both introduced and removed from the system continually.[32] This allows multiple measurements to be performed on the same sample without needing to modify the system or remove the sample. The Tian-Calvet system is especially well suited for adsorption studies because it directly measures the amount of heat generated from the adsorption event using heat flux sensors.[32] Since each data point represents a specific dose at a specific temperature at a specific loading, detailed structural information can be inferred from the isotherms generated using this system.

1.4 Motivation for Research

The research described in this thesis was intended to provide fundamental knowledge on both the structure and performance of MOFs by modifying the composition of metal clusters and functionalizing organic linkers. Research centered around two different classes of MOFs (single and multi-site), two different modification conditions (metal cluster and linker functionalization) and adsorbate polarity ranges for C_2 hydrocarbons. The first project sought to investigate the influence of adsorbate polarity and linker functionalization on a multi-site MOF, with low temperature measurements used to illustrate the multi-site adsorption model. The second project explored the effect of multiple metal sites within a single adsorption site MOF.

UiO-66 has become a widely researched MOF due to its stable, modifiable structure that has multiple adsorption sites and is stable in atmospheric conditions.[5-7,26-27,36] Due to

the difficulty of completing direct heat of adsorption measurements, most adsorption data for UiO-66 is derived from isosteric methods. As stated above, the isosteric method represents an average heat of adsorption over the multiple sites and yields no structural information.[32] Using the adsorption work of the Gorte group at the University of Pennsylvania as a model, we sought to establish a similar Tian-Calvet calorimeter to probe the effects of structure on adsorption activity. The second project was directly inspired by the Yaghi group at University of California at Berkeley, who were able to synthesize MOF-74 with a maximum of 10 different metals.[2] They found that inducing a single-phase system was difficult; metals accumulated in distinct regions within the nanocrystals and formed MOF aggregates.[2] Based on this, I designed a similar study where three common MOF-74 metals (cobalt, nickel and copper) were systematically mixed and assessed to establish whether phase rules could be used to design MOF systems and to isolate adsorption behavior of these mixed-metal samples.

The field of MOF research is relatively new, affording a wide variety of research topics to branch from a singular idea. PI Gross received a New Directions grant from ACS-PRF to fund research in a new field. Through this funding, I sought to build a new foundation of research with MOFs to expand the group's research capabilities and foster new connections in various departments at Wake Forest University.

2. UiO-66

2.1 Material Background

UiO-66 was an ideal MOF for this project due to its stable, multi-porous structure (Figure 2-1).[3] The MOF can accommodate functionalization, a high number of linker defects and has two distinct types of pores in its multi-pore structure. [26-27] In addition, UiO-66 is both moisture and thermally stable, making it an ideal candidate for industrial gas separations.[5-7,36]

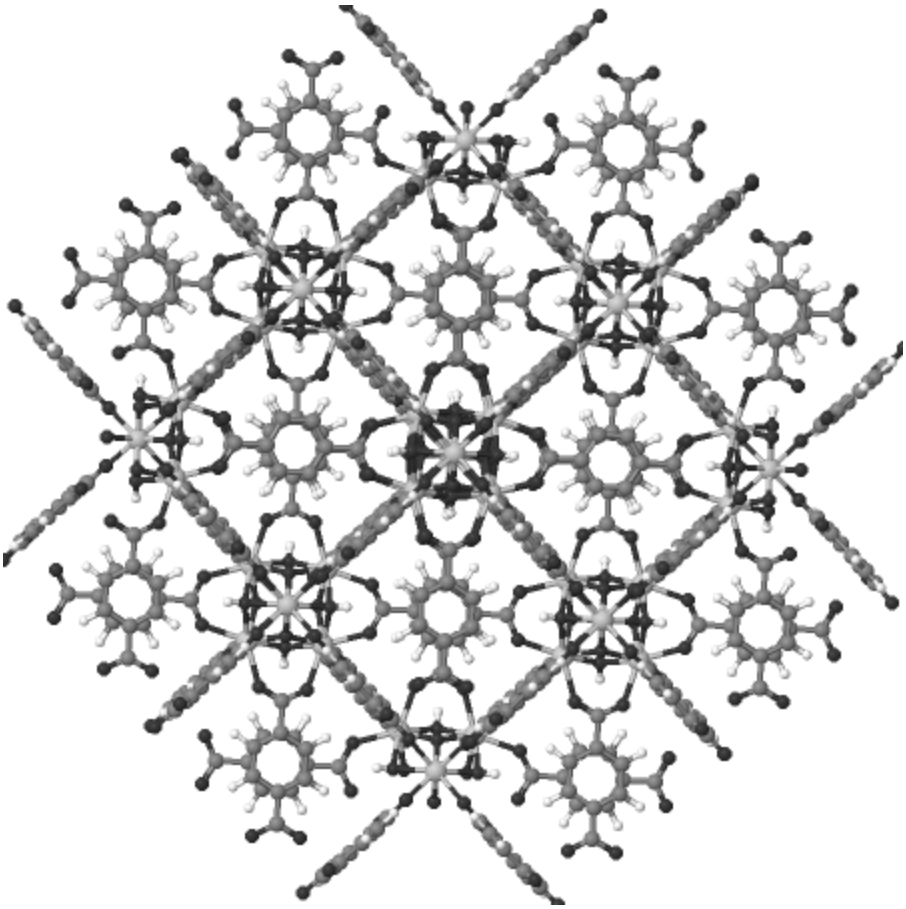

Figure 2-1: A line and ball structure of UiO-66 lattice structure. MOF is composed of Zr_6O_6 nodes and TPA linkers.[3]

The UiO-66 studies presented in Chapter 2 focus on dehydroxylated UiO-66, rather than the hydroxylated form of UiO-66, to avoid uncertainty associated with controlling the water content in the MOF.[37] The gas adsorption behavior on a standard UiO-66 structure was compared to adsorption on UiO-66 functionalized with either $–NH_2$ or $-NO_2$. The $–NH_2$ functional group is smaller and more polar than the $–NO_2$, allowing for comparison of adsorption heat due to polarity or confinement of the adsorbate.[13,21,38-39] Further, the number of defects in the UiO-66 was varied using an acetic acid

modulator, and the effect of defects on the adsorption behavior was assessed.[8] The gases studied were ethane, ethylene and acetylene to determine the primary factor driving the adsorption – electrostatic energy or size- of C_2 hydrocarbons on UiO-66 MOFs. A table of these factors is shown below.

Table I: A comparison of the electrostatic potential and kinetic diameters of the adsorbates used in these projects. Electrostatic potential was used to estimate relative polarity of the gas and kinetic diameter used to estimate relative size. [13, 21, 38-39]

Hydrocarbon	Formula	Structure	Electrostatic Potential (kJ/mol)	Kinetic Diameter (Å)
Ethane	C_2H_6		3.2	4.4
Ethylene	C_2H_4		7.5	4.2
Acetylene	C_2H_2		14.2	3.3

2.2 Synthesis and Preparation

For all samples produced, a 30 mL glass vial was filled with 20 mL DMF and 2 mL H_2O. The liquids were mechanically stirred before adding the dry reagents to the vial. A 1:1 molar ratio of $3.43 \cdot 10^{-4}$ mol organic linker (terephthalic acid) and $3.43 \cdot 10^{-4}$ mol metal salts was used for all synthesized samples. The linkers used were TPA (98%), TPA-NO_2

(99%) and TPA-NH_2 (99%) all obtained from Sigma Aldrich, with the metal salt $ZrCl_4$ (99.5%) obtained from Alfa Aesar. When inducing defects 1.32 mL of glacial acetic acid (99%) from Fisher was added with the liquids before the solids were added.

A solvothermal synthesis route was used for all samples. First, the liquid mixture was sealed and heated to 150 °C in a Vulcan 3-130 box furnace and held for twenty-four hours, then cooled to room temperature (25 °C) for two hours. Powder X-Ray Diffraction (PXRD) was used to verify the crystallinity of the MOF prior to washing.

Large-scale synthesis of the MOFs involved scaling up the above reactions 25x to theoretically produce 2g of MOF. In a 16 oz mason jar (437 mL), 200 mL DMF was added to 25 mL HAc and 25 mL HCl and manually stirred. The 1:1 molar ratio was preserved, using $8.58 \cdot 10^{-3}$ mol of both linker and metal. Samples were washed using a refluxing Soxhlet Extractor and a cellulose thimble. A first series of washes consisted of soaking in DMF to remove residual starting material and acid. The second series of washings was for solvent exchange, and samples were washed in HPLC-grade methanol continuously for a minimum of five days, with a solvent change occurring every three days to remove residual DMF. Washing was ceased when there was no more observable DMF layer suspended in the methanol wash. The MOF was removed from the air-dried thimble and pressed into a pellet (300 bar) using a hydraulic press. The pellet was then broken into pieces small enough to fit into the glass cell for calorimetry testing, a characteristic dimensional of ~5 mm. Once the MOF sample was loaded into the glass cell, glass beads were loaded on top

of the sample. The glass beads were added as an insulating barrier to heat flow during the calorimetry experiments. Secondarily, the glass beads mitigated any sample from being pulled out of the glass cell while pulling vacuum. Activation consisted of heating the sample to 180 °C in a Vulcan 3-130 box furnace while pulling vacuum on the sample for twenty-two hours. The sample cell was then filled with argon and then loaded into the calorimeter. The sample cell was filled with argon to prevent the sample from exposure to air because argon has a higher density than air. For calorimetry testing, the gases were tested in order of increasing theoretical heats of adsorption to avoid any potential irreversible binding events.

2.3 Experimental Work and Characterizations

Powder X-Ray Diffraction (PXRD) was completed with a Bruker D8 Desktop X-Ray Diffractometer to verify the crystalline MOF formed and the absence of starting material impurities. The 2θ range used was from 5°-30° with a 0.02° increment and 0.3 s time step, and the stage was rotated once per minute. Identity was verified using the first two peaks at approximate 2θ values of 7° and 9°. A sample XRD is shown in Figure 2-2:

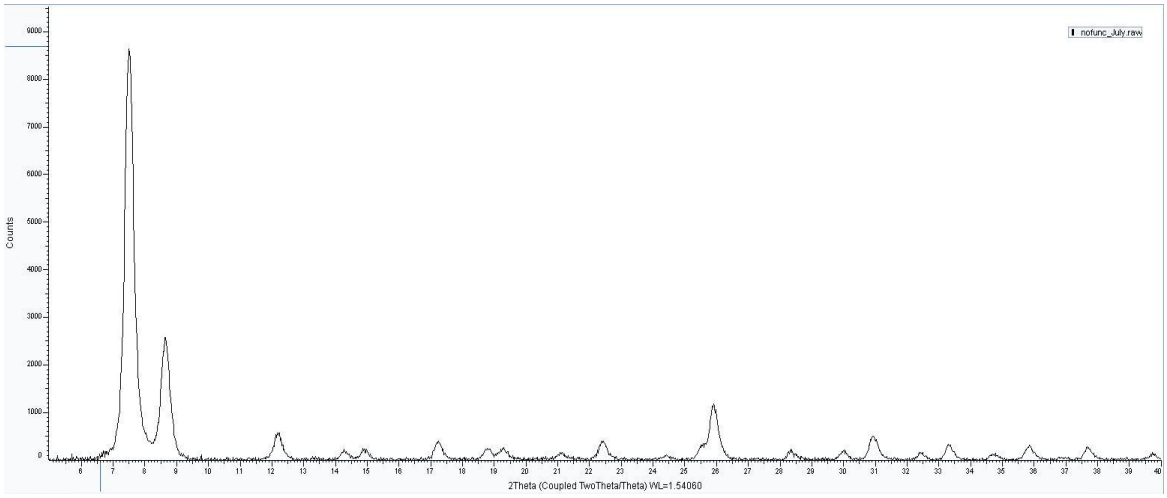

Figure 2-2: An example XRD pattern used to verify the UiO-66 crystallinity prior to loading.

The Tian-Calvet calorimeter (Figure 1-3) was a home-built system for the direct measurement of heats of adsorption. The sample cell was surrounded by 1 sq.in. heat flux sensors on 5 sides. The heat flux sensors used were C-LT-1 Thermal Flux meters from ITI Corporation. The pressure gauges used were the Instrutech Micro Bee gauges connected to Cen-Tech digital multimeters, the signal amplifier used was an Omega Omni Amp III and heat flux multimeter used was a Keithley 2100 6 ½ digit multimeter. A 5 kg aluminum block served as an isothermal heat sink for the heat generated during the adsorption events. The heat sink, sensors and cell were located under the gas handling system in a Styrofoam container. The Styrofoam container was insulated to maintain isothermal conditions and prevent errant drafts of air from affecting the heat flux sensor readings. Gas adsorption measurements were collected at 293 K and 195 K. During low temperature readings, the Styrofoam container was filled with dry ice; the dry ice was refilled as needed to maintain the isothermal condition. Adsorbates were dosed into the sample cell in controlled amounts

between 50-750 torr. Once the sample was dosed with a gas adsorbate, the heat flux sensors generated a voltage as a function of time signal; an example is shown in Figure 2-3:

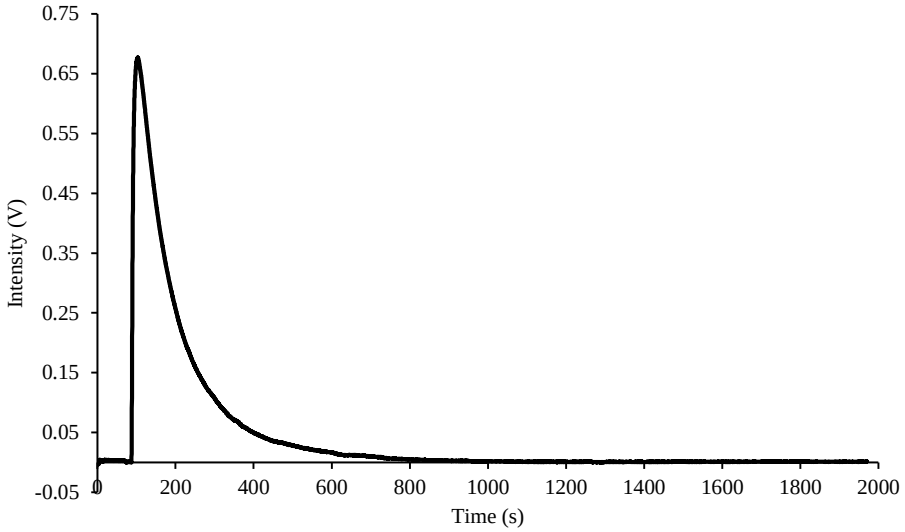

Figure 2-3: An example of the normalized data graph generated by the multimeter during and following the adsorption event. The area under the curve directly relates to the differential energy of the adsorbate. Graph taken from UiO-66 S1 acetylene dose 5

Samples were held under vacuum overnight after loading into the calorimeter, then the voltage was allowed to stabilize for 30 minutes before the first adsorbate dose. When recording data, a minimum 60 second baseline was established before dosing the adsorbate to the system. Data was recorded until the signal reached a steady baseline, normally after 30-40 minutes.

For defect-induced samples, TGA analysis was going to be used to corroborate the actual number of missing linkers per metal cluster. Due to external circumstances, this was

not able to be completed before the data was due. The defect-induced sample had a larger interior pore volume than the normal sample. Katz et al.[25] has indicated that open pore volume can be used to calculate the approximate number of linker defects per metal site. Using this information, I was able to say that the normal sample (S1) has approximately one missing linker per twelve coordinated ones, while the defect-induced sample (S5) has approximately four missing linkers out of twelve.

2.4 Results and Discussion

The following results explore the effects of linker functionalization, ambient temperature and linker defects on the adsorption behavior of C_2 hydrocarbons. Important structural information was also found and inferred during these trials.

2.4.1 Effects of Functionalization of Linker on Adsorption Activity

The following isotherms (Figures 2-4: 2-6) compare the effect of functionalization on adsorbate activity at room temperature:

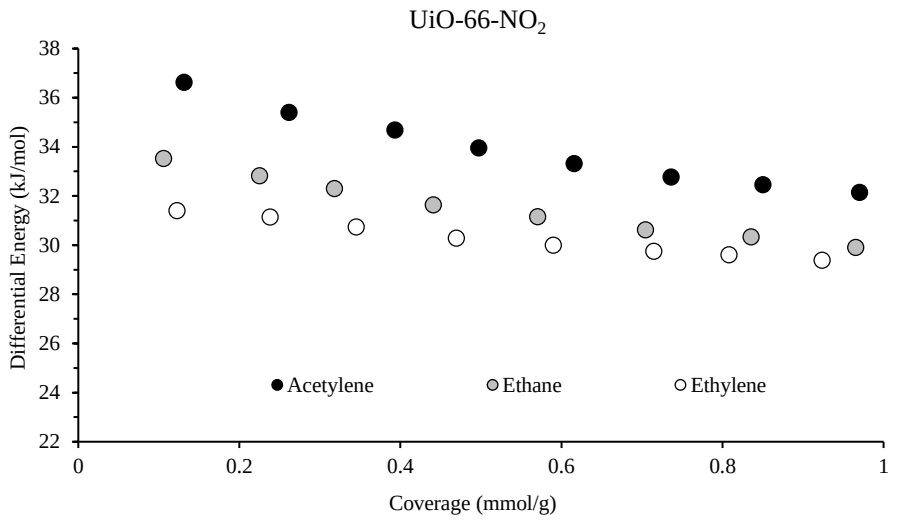

Figure 2-4: The differential adsorption energy of C_2 hydrocarbons on UiO-66-NO_2

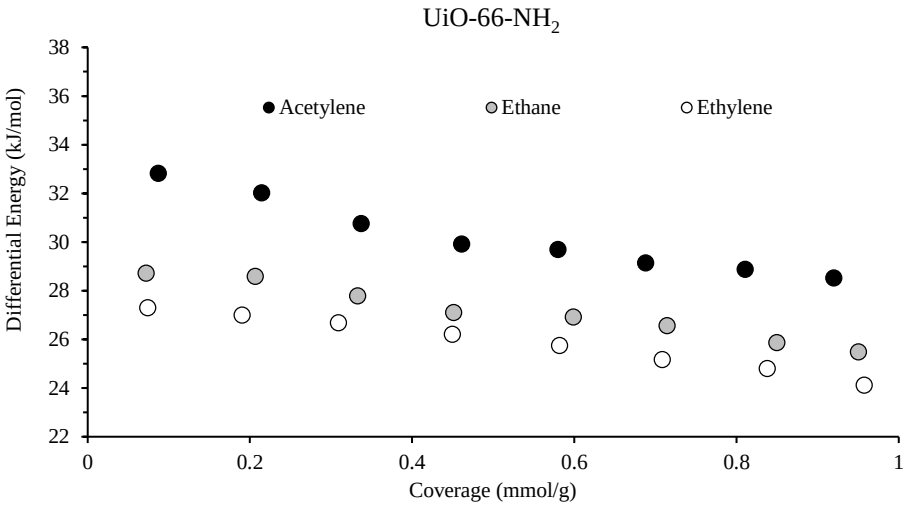

Figure 2-5: The differential adsorption energy of C_2 hydrocarbons on UiO-66-NH_2

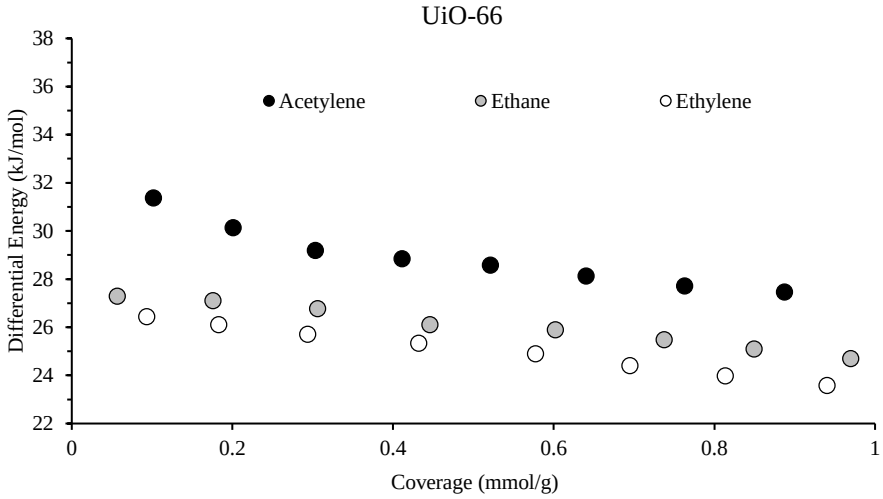

Figure 2-6: The differential adsorption energy of C_2 hydrocarbons on UiO-66

Binding energies for functionalization followed the pattern *UiO-66-NO_2 > UiO-66-NH_2 > UiO-66*. Binding energies for the adsorbates followed the pattern *acetylene > ethane > ethylene.*

In all cases, the -NO_2 functionalization showed the highest heat of adsorption followed by -NH_2, with the non-functionalized sample showing the lowest heat values. This indicates that confinement effects at the binding site dominates during the binding event more than polarity of the binding site, but that both factors play a key factor in adsorbate behavior in the lattice. In terms of adsorbate behavior, acetylene had the highest differential energy of all C_2 hydrocarbons studied, followed by ethane and then ethylene. This is an interesting scenario; the polarity of acetylene dominates binding energy but is then followed by the bulky ethane, with ethylene having the lowest energy of the group.

This suggests the polarity of ethylene does not significantly impact adsorption behavior while the size of ethane does. Our group is currently in collaboration with the Thonhauser group to gain more insight into these results with computational modeling.

2.4.2 Effects of Temperature on Adsorption Activity

The following isotherm (Figure 2-7) compares the adsorption behavior of C_2 hydrocarbons on UiO-66-NO_2 at dry ice temperature:

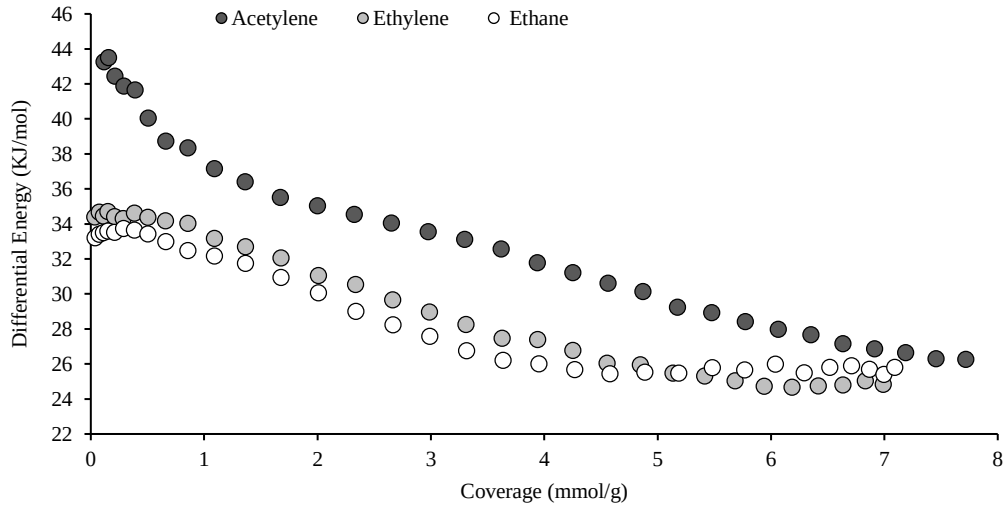

Figure 2-7: A comparison of acetylene, ethylene and ethane on UiO-66-NO_2 at 195K.

Collecting measurements at 195 K provides additional insights into the adsorption behavior of C_2 hydrocarbons on the MOF. UiO-66-NO_2 was able to achieve nearly four times more coverage at the same loading for gases at low temperatures versus room temperature. Both ethane and ethylene showed a solid starting plateau, a decrease in

binding energy and a second plateau in terms of isotherm shape. This indicates a multi-site binding model in which there is a strong, high heat binding site and a weaker, low heat binding site. This information is consistent with the multi-pore shape of UiO-66-NO_2.

Acetylene binding on UiO-66-NO_2 showed exceptionally high heats of adsorption at very low coverages (below 0.5 mmol/g). This suggests that there may be a small concentration of a third type of binding sites with an extremely high binding energy. There are two possible explanations of this behavior. First, the results could be due to a small concentration of missing linker defects. While no attempt was made to induce missing linker defects in the samples, the literature shows that it is quite difficult to eliminate all missing linker defects [40-42]. Second, the literature shows that some research groups include additional processing steps of the acetylene prior to adsorption. Specifically, the acetylene is flowed over molecular sieves and activated carbon to remove any possible residual acetone in the acetylene [43-44]. The follow-up to these results are detailed in section 2.4.3 below.

2.4.3 Effects of Linker Defects on Adsorption Activity

The following isotherm (Figure 2-8) compares the effect of induced linker defects of UiO-66 on acetylene binding at low temperatures:

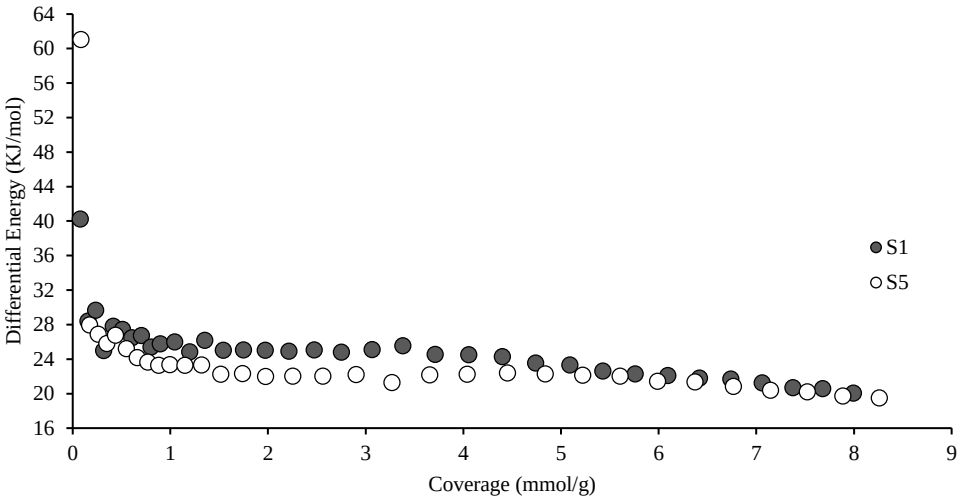

Figure 2-8: A comparison of the adsorption energy of acetylene on UiO-66 with none/induced defects at 195K.

Prior to the completion of this isotherm, GC-MS measurements indicated that acetone accounted for less than 3% of the total composition of the acetylene gas used; Both S1 and S5 indicated the same high binding energy at low concentrations. For S1, with an estimated one linker defect, this value was 41 KJ/mol followed by a plateau at 29 KJ/mol; S5 has an estimated four linker defects and had an initial value of 62 KJ/mol followed by a plateau at 28 KJ/mol. Calculations indicate that the initial high heat of adsorption value could not be caused by the acetone impurity because it only comprises 3% of the dosed gas. The acetylene results suggest the presence of a third type of binding site; whether it is due to missing linker defects is still not resolved. We are currently working with the Thonhauser group for explanations through computational modeling.

2.5 Proposed Future Work

Future work building on these projects should focus on expanding the gas variety tested on the functionalized MOF and completing more low coverage measurements for some UiO-66 samples. Small dosing intervals at low coverages will further isolate specific site interactions within the lattice, helping to explain the high heat phenomenon. In addition, expanding the range of gasses to include larger and smaller hydrocarbons, along with some other industrially relevant gasses, will may provide additional insight to elucidate the importance of polarity versus size in MOF binding behavior, while also further exploring the industrial relevance of UiO-66.

Along with computer modeling, further experiments should be completed to further explore the role of linker defects in UiO-66. Firstly, replicating the data for S1 and S5, but with smaller loading intervals at low coverage would likely provide more insight into the low coverage behavior and the third type of adsorption site. The data above represents a single run of each sample and since the data is so unusual, further isotherms need to be generated to confirm it was not caused by other unrelated factors. New samples of S1 and S5 will ensure a good starting point and be guaranteed to not have any leftover adsorbate on the lattice. A molecular sieve and activated carbon tube should also be fitted to the tanks to remove any residual acetone, so all results can be attributed solely to acetylene binding on the lattice. Coupling future isotherms with models of UiO-66 defect behavior should elucidate this phenomenon.

3. MOF-74

3.1 Material Background

MOF-74 was chosen for this project due to the ease with which various metals can be substituted into the metal clusters of the structure.[2] Further, MOF-74 has a simplistic structure and synthesis method, making it ideal for interpreting the effect of metal substitution in the metal cluster. A lattice structure is shown in Figure 3-1:

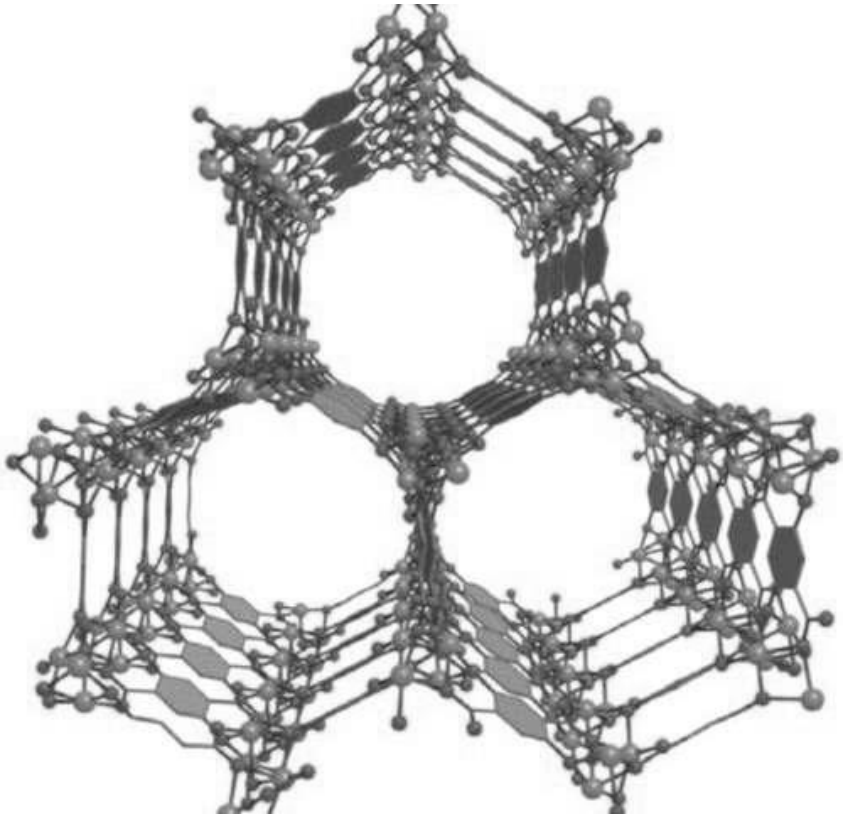

Figure 3-1: A line and ball structure of MOF-74 lattice structure. MOF is composed of M_3O_3 clusters and H_4DOBDC linkers [45].

MOF-74 was synthesized with cobalt, nickel, copper and bimetallic combinations of the three metals. The metals were selected based on solid-state solubility to test both one- and two-phase metal systems. Based on solid state solubility rules (Hume Rothery rules) , both Co-Ni and Ni-Cu systems form a single-phase solid solution, while Co-Cu are insoluble, forming a two-phase metal system. The solubility of the metals could be significant in the adsorption behavior of MOF-74 because it has a metal "backbone" extended throughout the structure, which serve as the primary adsorption sites (Figure 3-1). The metals are directly connected to each other in the structure, meaning the system can either follow one of two scenarios: the metals will form the connected metal cluster structure with no discrimination of metal site occupation or the rods will exclusively form with singular metal types. A wider variety of gases beyond C_2 hydrocarbons (methane, ethane, ethylene, acetylene and carbon dioxide) were tested on the MOF-74 samples to more fully assess the role of metal content on adsorption behavior.

Over the course of this project, we attempted to identify the location of metal atoms within the structure using single crystal x-ray diffraction (SCXRD). There have been very few published methods of growing single-crystal samples of MOFs that are large enough for this type of analysis.[46-47]

3.2 Synthesis and Preparation

For all samples produced, a 30 mL glass vial with lid was filled with a 15:1:1 DMF: H_2O: EtOH volumetric (mL) ratio. The liquids were mechanically stirred before adding the

dry reagents to the vial. A 3:1 molar ratio of metal: linker was used, $1.5 \cdot 10^{-4}$ moles of linker and $4.5 \cdot 10^{-4}$ moles of metal worked well with the volumetric amounts selected. The organic linker was H_4DOBDC (97%) and the metal salts used were nickel nitrate hexahydrate (98%), cobalt nitrate hexahydrate (98%), and copper nitrate hemi-pentahydrate (98%). All reactants were purchased from Alfa Aesar. To more accurately predict the molar ratio of metal precursors required to achieve a particular metal ratio concentration in the MOF, a calibration curve of final metal content in the MOF as a function of initial molar amounts of metal salts was created using ICP-MS analysis. The calibration curve was used for all subsequent synthesis calculations, to determine molar amounts of metal needed for final desired content. Figure 3-2 illustrates this below:

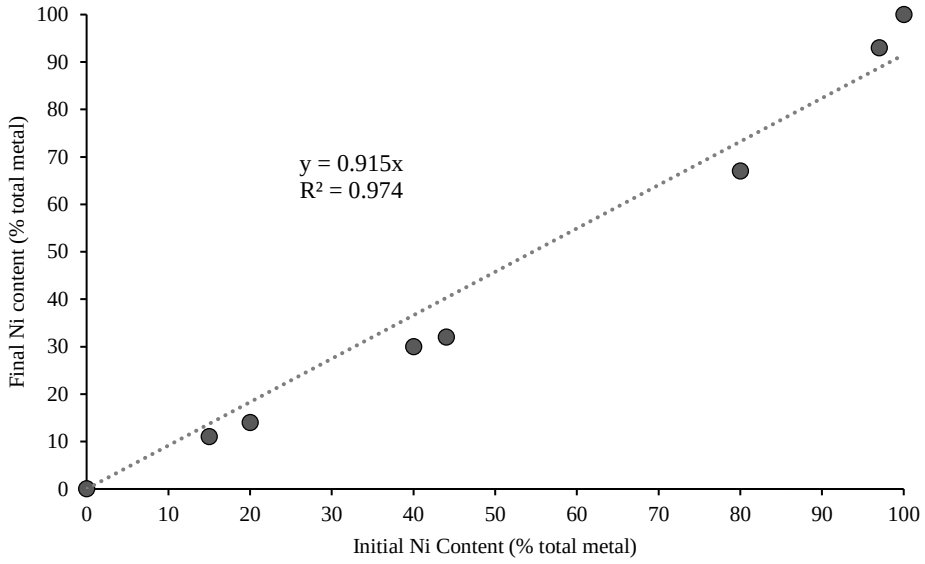

Figure 3-2: A molar comparison of nickel added to the initial Co-MOF-74 solution to the nickel present in the final Co-Ni MOF-74.

A solvothermal synthesis route was used for all samples. First, the liquid mixture was sealed and heated to 120 °C in a Vulcan 3-130 box furnace and held for twenty-two hours, then cooled to room temperature (25 °C) in 2 hours. PXRD was used to verify the crystallinity of the MOF prior to washing.

Large scale synthesis of the MOFs involved scaling the above reaction by a factor of 13, to produce a theoretical 2g of material. 200 mL DMF and 13 mL H_2O and EtOH were placed in a 16 oz mason jar (473 mL). The same 3:1 molar ratio was preserved, using $5.85 \cdot 10^{-3}$ mol linker and $1.95 \cdot 10^{-3}$ mol metal salt in each trial. Samples were washed using a refluxing Soxhlet Extractor while contained in a cellulose thimble. A first series of washes consisted of soaking in DMF for three days to remove residual starting material. The second washings were for solvent exchange, and samples were washed in HPLC-grade methanol continuously for a minimum of five days, with a solvent change occurring every three days to remove residual DMF. Washing was ceased when there was no more observable DMF suspended in the methanol wash. The MOF was removed from the dried thimble, pressed into a pellet (300 bar), broken into pieces, and then loaded into a glass cell for activation. Glass beads were loaded in the cell on top of the MOF to keep the sample stationary while vacuum was pulled. Activation consisted of heating the sample to 250°C in a Vulcan 3-130 box furnace while pulling vacuum on the sample for twenty-two hours. The sample cell was subsequently loaded into the calorimeter and tested in order of increasing theoretical adsorption energies of gases.[48]

3.2.1 Single-Crystal Growth Methods

There are three main factors that affect crystal growth: temperature, time, and the mother liquor the crystal is grown in. Synthesis was completed with the same molar and volumetric ratios in a 30 mL vial, similar to that described above. A 43:57 molar ratio of Co: Ni was used to achieve an equimolar final mixture, based on the calibration curve above. Synthesis temperature was first adjusted to ramp to 90°C for 60 hours, which produced small crystalline flakes. Next, modulator ($1.47 \cdot 10^{-4}$ mol BZA) was added to the mother liquor and heated at 90 °C for 60 hours, producing crystalline starting material (H_4DOBDC and metal salts). Campbell et al.[47] suggested the starting liquor polarity and hydrogen bonding was responsible for larger crystals, so focus shifted away from temperature and towards systemically altering ratios of DMF: H_2O: EtOH from 15:1:1 (v) to a more polar, less organic ratio. Crystal seeding, or using an existing crystal as a scaffold for future crystal growth, was introduced in conjunction with this work. A sample seeded with a BZA flake in a 15:1:1 of DMF: H_2O: EtOH solvent was unsuccessful. Synthesis with a 10:5:5 of DMF: H_2O: EtOH solvent produced cylindrical 4μm long crystals, which were too small to analyze. A further sample seeded with these small crystals yielded no suitable crystalline product. Modifying the volumetric ratio to 6:7:7 of DMF: H_2O: EtOH produced single crystal quality crystals in terms of size and purity. However, the crystals consistently grew twinned; one crystal plane grew over another, making SCXRD impossible. Removing DMF from the mother liquor entirely (1:1 of H_2O: EtOH) produced no crystals, illustrating the non-polar solvent was essential for full dissolution and integration of the organic linker into the matrix. Replacing DMF with a similar organic solvent (butanol) in a 6:7:7 volumetric ratio did not produce adequate crystals for analysis.

The only successful single crystal synthesis utilized a 6:7:7 volume ratio of DMF: H_2O: EtOH, held at 90 °C for 21 hours and cooled overnight. These crystals were consistently twinned through subsequent trials. No further attempts to produce suitably sized single crystal was pursued.

3.3 Experimental Work and Characterizations

PXRD completed on the Bruker D8 Desktop was used to verify the MOFs formation and absence of starting material prior to calorimetry. The 2θ range used was from 5°-40° with a 0.02° increment and 0.3 s time step, with the stage rotating once per minute. Phase identity was verified using the first two peaks at approximate points 6° and 12°. A sample XRD is shown in Figure 3-3:

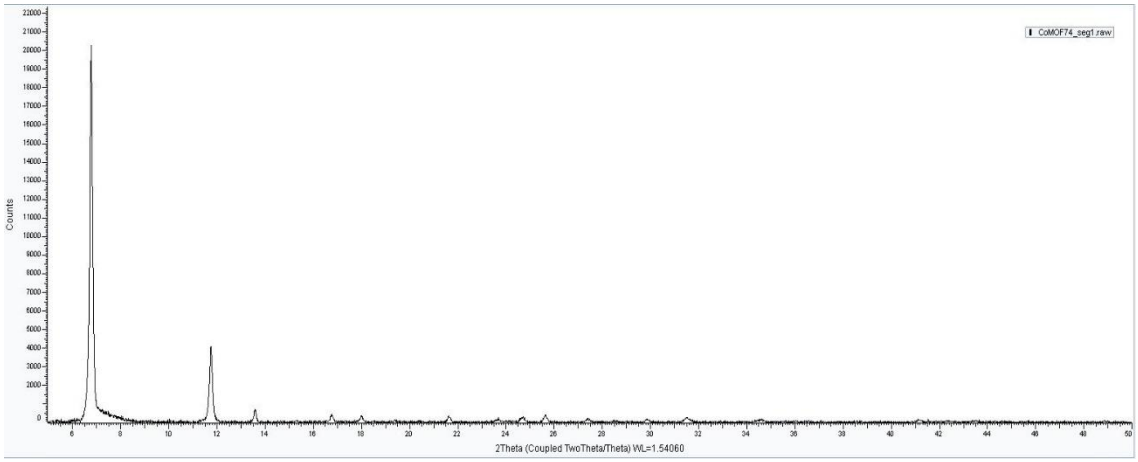

Figure 3-3: An example XRD pattern to verify MOF-74 crystallinity prior to loading.

The Tian-Calvet calorimeter was built in-lab to support direct energy measurements. The heat flux sensors used were C-LT-1 Thermal Flux meters from ITI, the pressure gauges used were Instrutech Micro Bee gauges connected to Cen-Tech digital multimeters, the signal amplifier used was an Omega Omni Amp III and the multimeter used was a Keithley 2100 6 ½ digit multimeter. The sample cell was surrounded by 1 sq.in. heat flux sensors on 5 sides. A 5 kg aluminum block acted as a heat sink to these sensors. The heat sink, sensors and cell were located under the main gas dosing apparatus, insulated and wrapped to prevent errant drafts from affecting the heat readings. Adsorbate was dosed into the sample cell in small, controlled amounts to ensure accurate pressure and voltage readings from the multimeters. The heat flux sensors generated a voltage vs time graph; an example is shown in Figure 3-4:

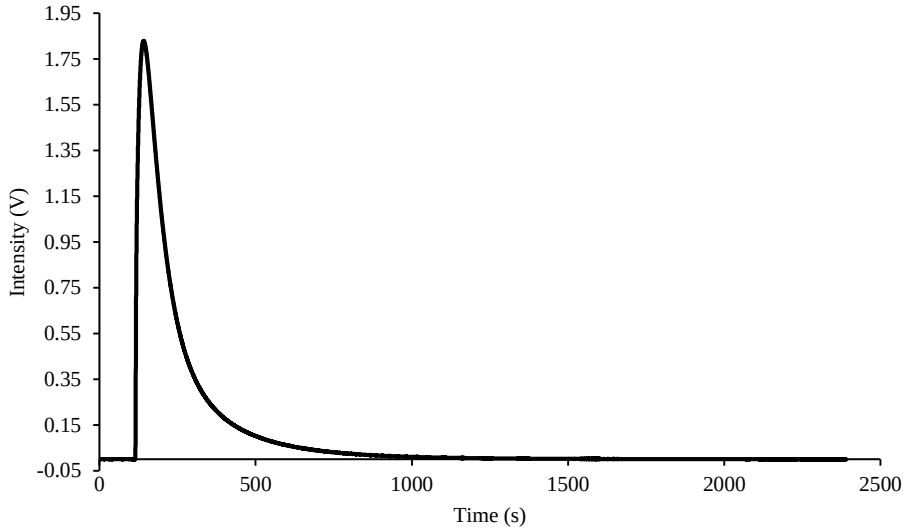

Figure 3-4: An example of the normalized data graph generated by the multimeter during and following the adsorption event. The area under the curve directly relates to the differential energy of the adsorbate. Graph taken from Co-MOF-74 acetylene dose 4.

Samples were pulled to a full vacuum overnight after loading into the calorimeter, then the voltage was allowed to stabilize for 30 minutes before the first data point was taken. When recording data, a minimum 60 second voltage baseline was recorded before introducing the adsorbate to the system. Data was recorded until the system resolved back to baseline, normally after 25-30 minutes. The voltage graph was normalized to a zero baseline before data analysis began. The voltage was converted to joules using the calibration value obtained from the manufacturer of the heat flux sensors. The area under the voltage curve was used to directly calculate the energy released by the adsorbate during the adsorption event.

One interesting factor noted was that the color of the MOF was affected by water content. Freshly synthesized (water present) Ni-MOF-74 was a bright yellow color that became wood-brown during the activation process (water removed). After all testing was completed and the sample was unloaded from the calorimeter, being exposed to atmospheric humidity, it slowly turned yellow over a day. Similar experiences were recorded with both Co-MOF-74 and Cu-MOF-74.

3.4 Results and Discussion

The following Table I compares the theoretical heats of adsorption with the experimental heats of adsorption for both pure and mixed-metal MOF-74 samples. For

data sets without a clear plateau, the average of the first 3 points, barring any outliers, was used.

Table II: A comparison of theoretical binding energies and the measured direct binding energies of carbon-containing gases on MOF-74 synthesized with pure and mixed metal compositions.[48]

		Methane	Ethane	Ethylene	Acetylene	CO_2
Co	Theoretical	18	35	38	36	34
	Experimental	16.5	30	43.5	42.5	33
Ni	Theoretical	19	36	41	37	37
	Experimental	17	29	45.5	51	37
Cu	Theoretical	14	27	22	20	27
	Experimental	10.5	21	24	25.5	17.3
Co-Ni	Theoretical	18-19	35-36	38-41	36-37	34-37
	Experimental	15	29	46	42	36
Ni-Cu	Theoretical	14-19	27-36	22-41	20-37	27-37
	Experimental	9.6	21.5	25.5	28.6	21
Co-Cu	Theoretical	14-18	27-35	22-38	20-36	27-34
	Experimental	8.5	19	25.5	29.3	23

As shown in Table 1, the experimental differential heats of adsorption varied from theoretical. For methane and ethane gases, the theoretical values were always higher than experimental. Ethylene and acetylene had higher experimental energies than theoretical values. CO_2 values were consistent with cobalt and nickel samples, and lower in copper containing samples. One thing to note is that the saturated hydrocarbon gases (methane and ethane) had lower values while unsaturated hydrocarbons (ethylene and acetylene) had higher values compared to theoretical.

The following isotherms (Figures 3-5: 3-7) compare the effects of metal content on the adsorption behavior of methane:

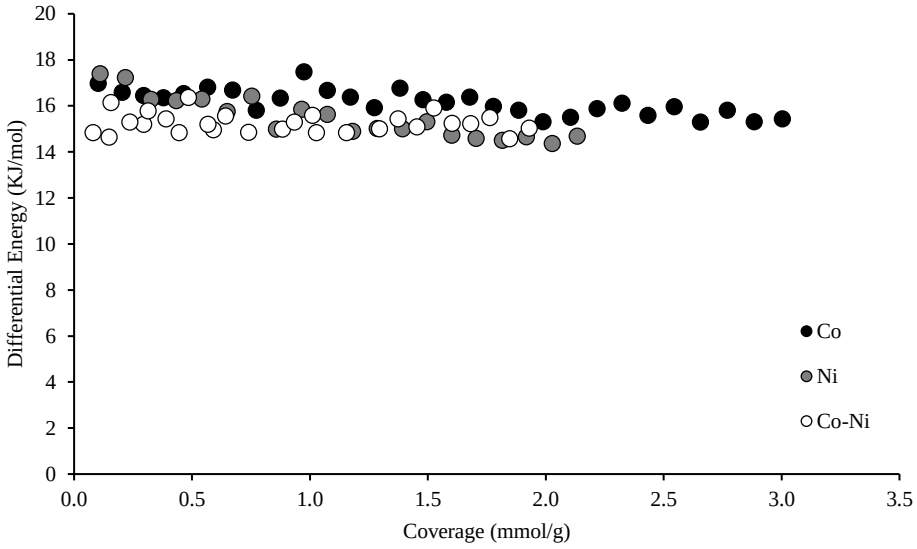

Figure 3-5: The differential adsorption energy of methane on pure Co, Ni and mixed-metal MOF-74

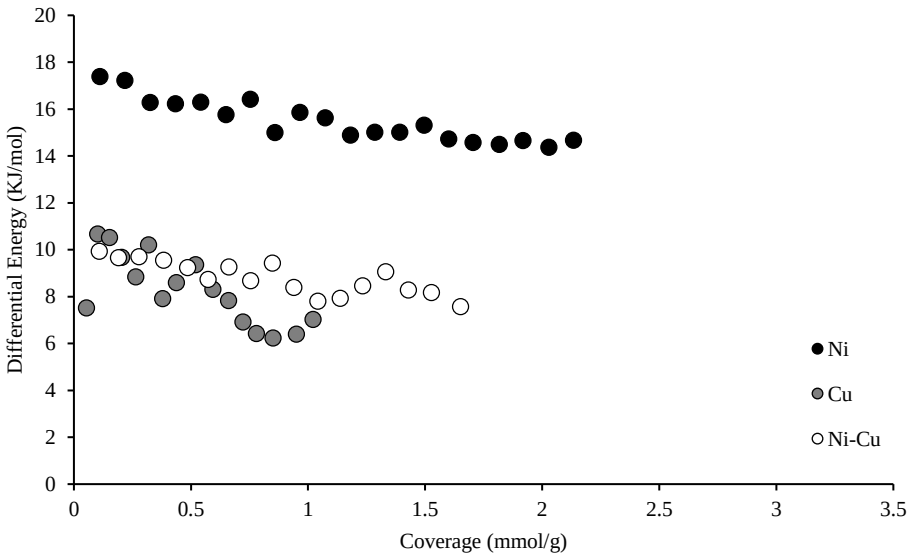

Figure 3-6: The differential adsorption energy of methane on pure Ni, Cu and mixed-metal MOF-74

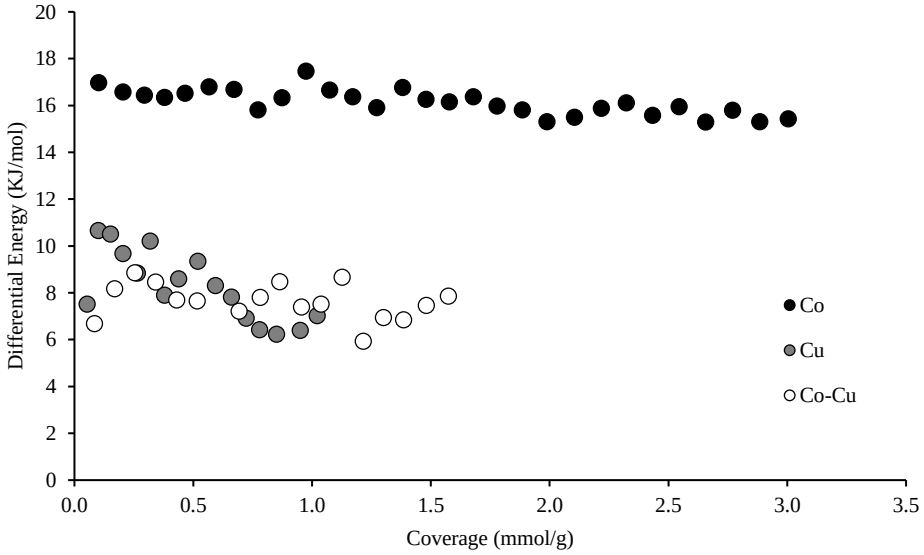

Figure 3-7: The differential adsorption energy of methane on pure Co, Cu and mixed-metal MOF-74

Both the pure cobalt and pure nickel samples had relatively flat shapes to their isotherms and showed consistent heat behavior over the range of coverage studied. The

copper containing samples had more variation in the binding energies and lower coverages overall.

The following isotherms (Figures 3-8: 3-10) compare the effects of metal content on the adsorption behavior of ethane:

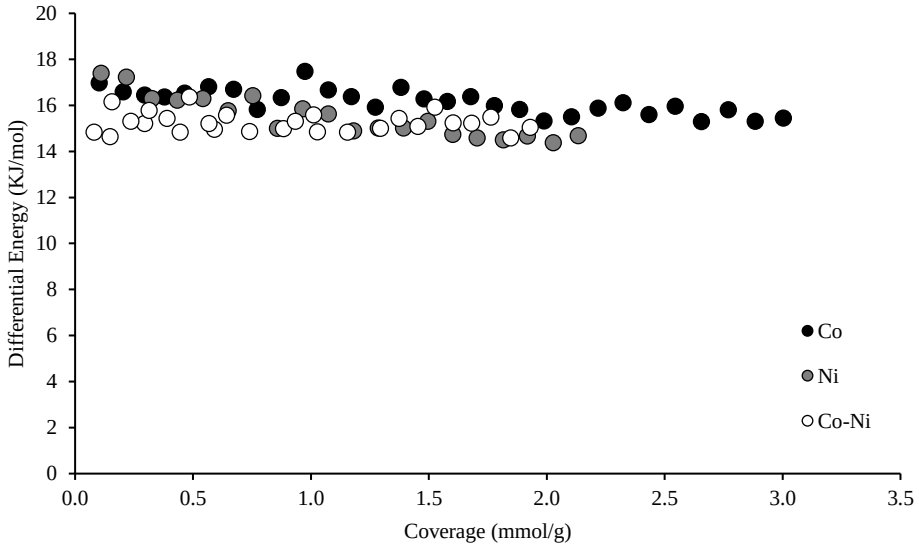

Figure 3-8: The differential adsorption energy of ethane on pure Co, Ni and mixed-metal MOF-74

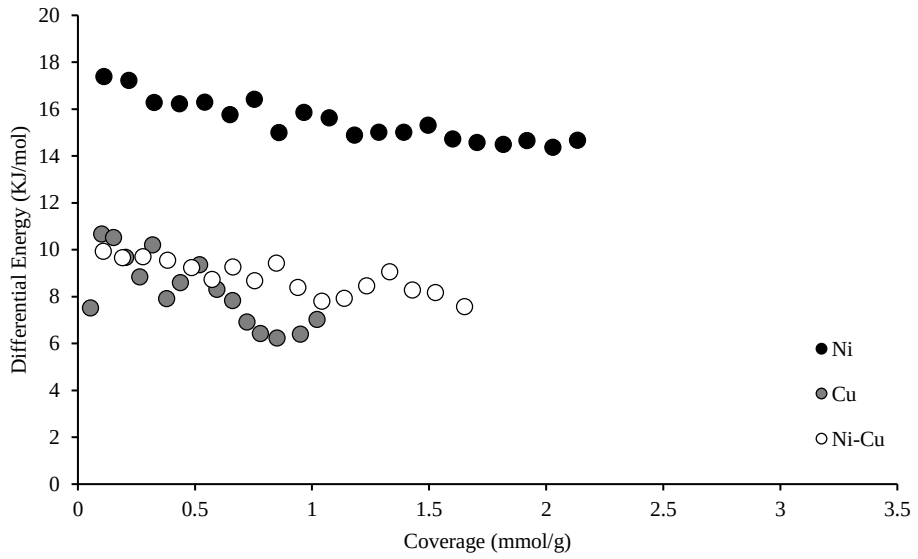

Figure 3-9: The differential adsorption energy of ethane on pure Ni, Cu and mixed-metal MOF-74

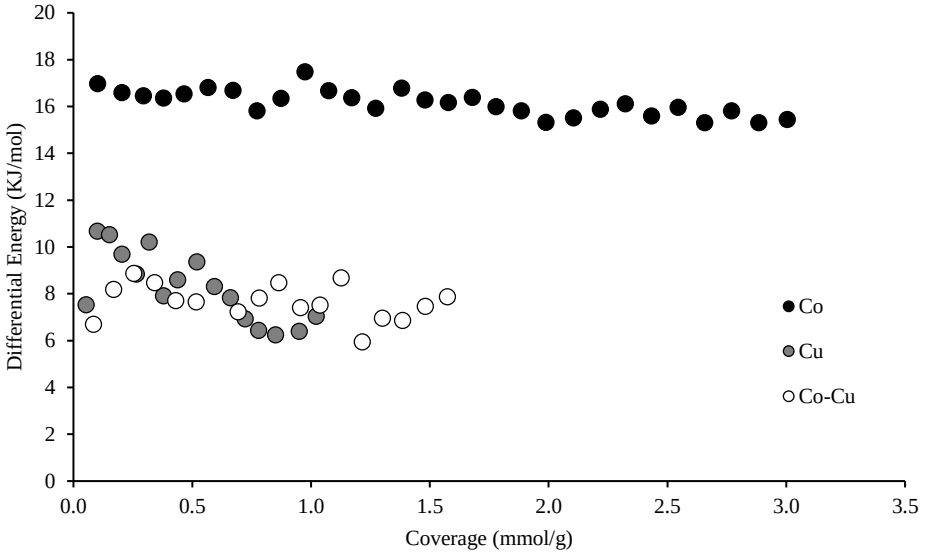

Figure 3-10: The differential adsorption energy of ethane on pure Co, Cu and mixed-metal MOF-74

Both the pure cobalt and pure nickel samples had relatively flat shapes to their isotherms and showed consistent heat behavior over the coverage, much like the methane results. Also similar to the methane results, coverage did not exceed 3.5 mmol/g. This is a

low range compared to other gases on MOF-74. Both ethane and methane are bulky, non-polar gases, indicating electrostatic potential has a significant effect on gas adsorption. The copper containing samples again showed more noise in the binding energies and lower coverages overall.

The following isotherms (Figures 3-11: 3-13) compare the effects of metal content on the adsorption behavior of ethylene:

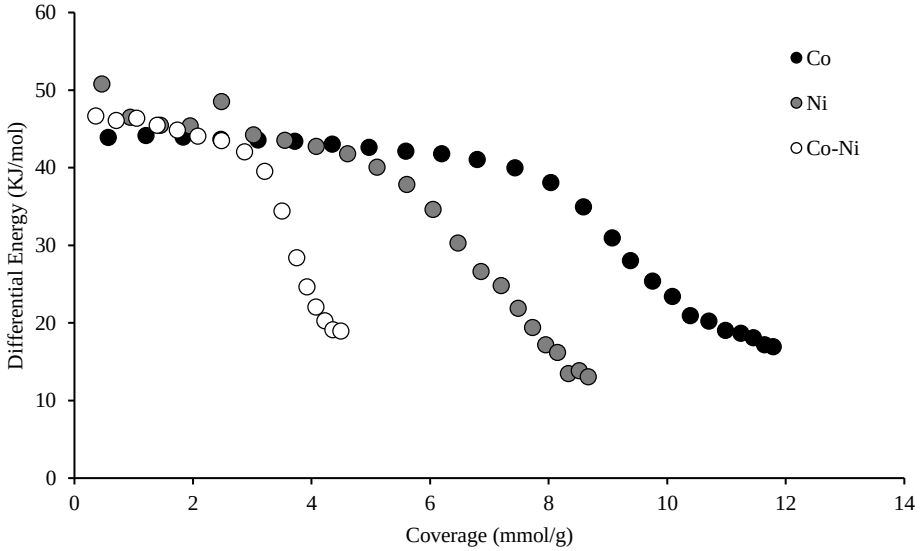

Figure 3-11: The differential adsorption energy of ethylene on pure Co, Ni and mixed-metal MOF-74

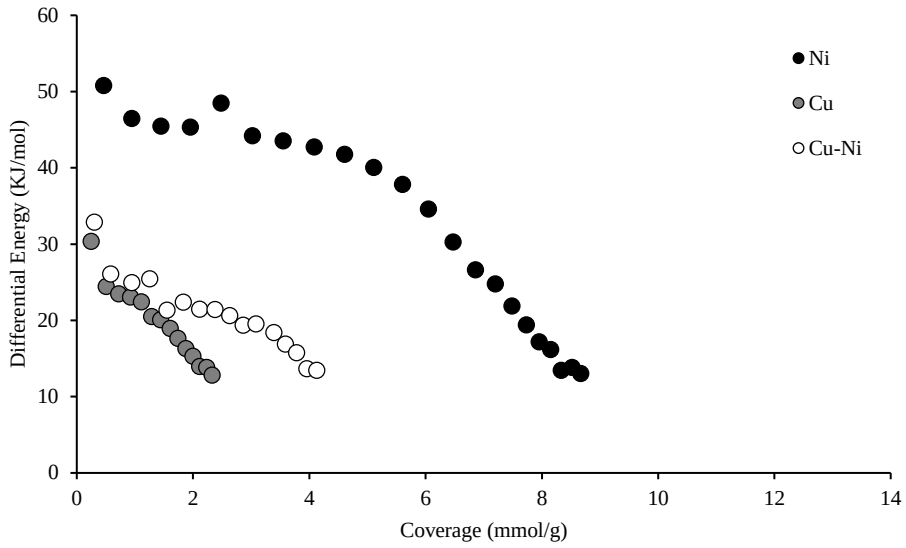

Figure 3-12: The differential adsorption energy of ethylene on pure Ni, Cu and mixed-metal MOF-74

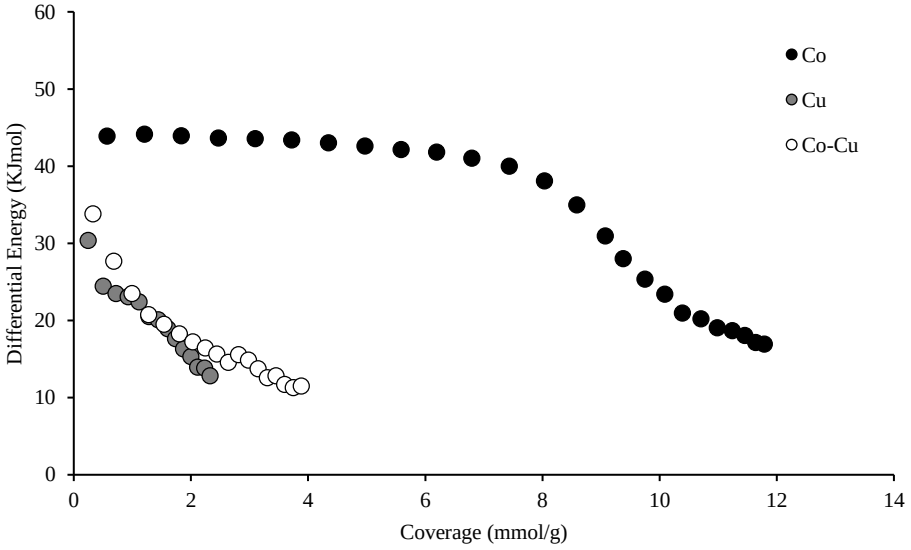

Figure 3-13: The differential adsorption energy of ethylene on pure Co, Cu and mixed-metal MOF-74

Coverages and heats for the MOFs were much higher with ethylene compared to methane and ethane, indicating a stronger binding interaction between ethylene and the MOF. The heat of adsorption for Co-MOF-74 showed a large initial plateau with consistent differential heats. Ni-MOF-74 had a more negative slope to the heats as a function of coverage compared to Co-MOF-74, and Cu-MOF-74 exhibited to most negative slope for heat as a function of coverage. The cobalt containing sample had 3x more coverage per gram than the copper MOF. In addition, the heat of adsorption profile for Cu-mixed metal MOFs both matched the profile of pure Cu-MOF.

The following isotherms (Figures 3-14: 3-16) compare the effects of metal content on the adsorption behavior of acetylene:

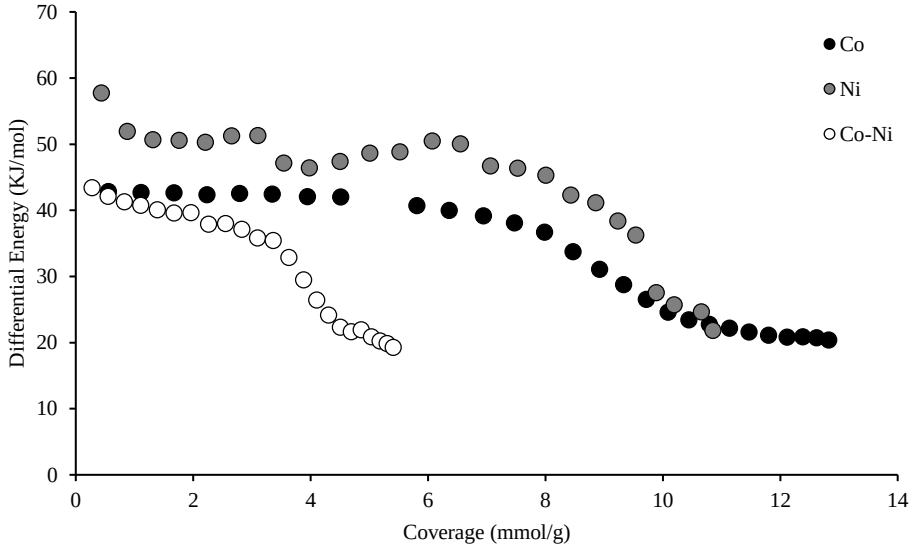

Figure 3-14: The differential adsorption energies of acetylene on pure Co, Ni and mixed-metal MOF-74

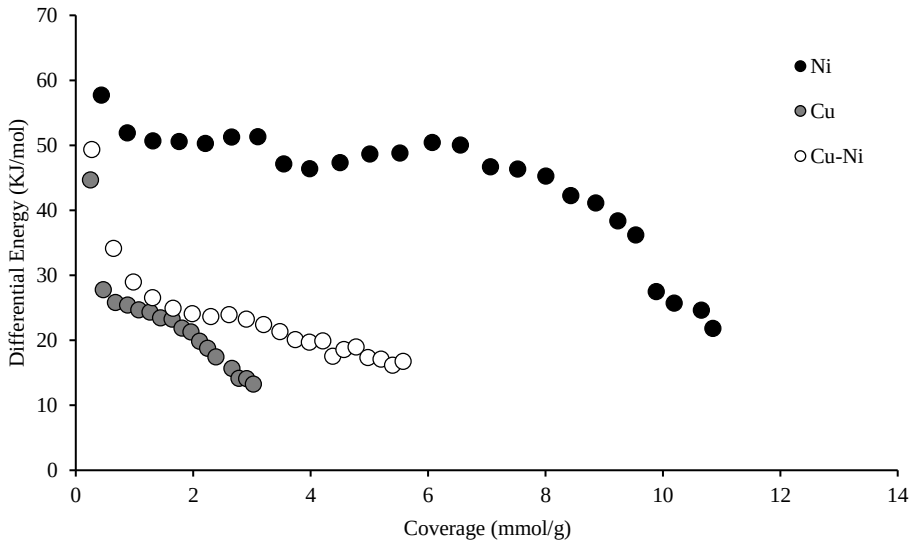

Figure 3-15: The differential adsorption energies of acetylene on pure Ni, Cu and mixed-metal MOF-74

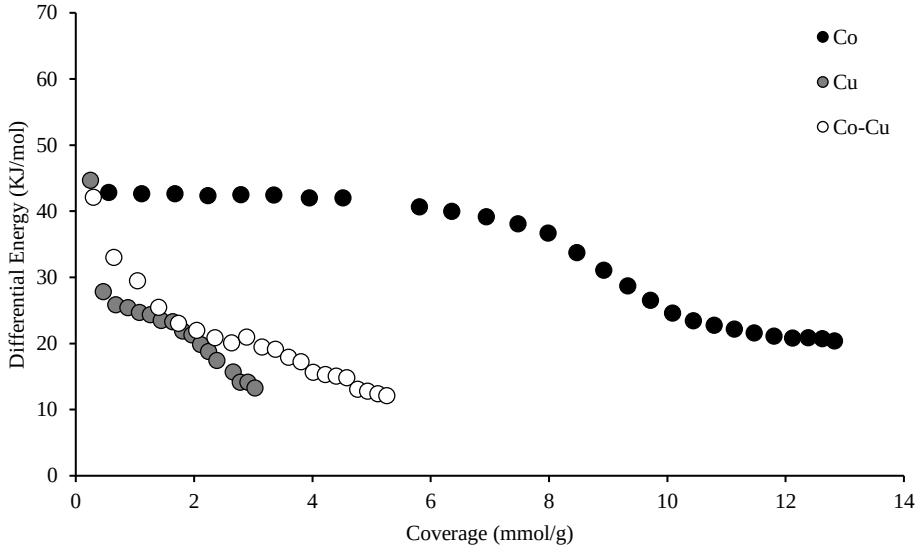

Figure 3-16: The differential adsorption energies of acetylene on pure Co, Cu and mixed-metal MOF-74

Both nickel and copper containing MOFs showed an initial high heat of adsorption. In the case of Cu, the heat of adsorption decreases sharply with increasing coverage. For Co-MOF-74, the heat of adsorption is consistent over a wide range of coverage. In these

trials, the Ni-MO-74 had higher differential energies than the Co-MOF-74, unlike the hydrocarbon gases seen previously. Previously, pure Co-MOF-74 had higher adsorption heats, yet Ni-MOF-74 showed a nearly 10 KJ/mol higher value with acetylene. Consistency with multiple points on the isotherm indicated the high heat is not the result of external influences. This is both unexpected and unusual behavior for the sample.

The following isotherms (Figures 3-17: 3-19) compare the effects of metal content on the adsorption behavior of CO_2:

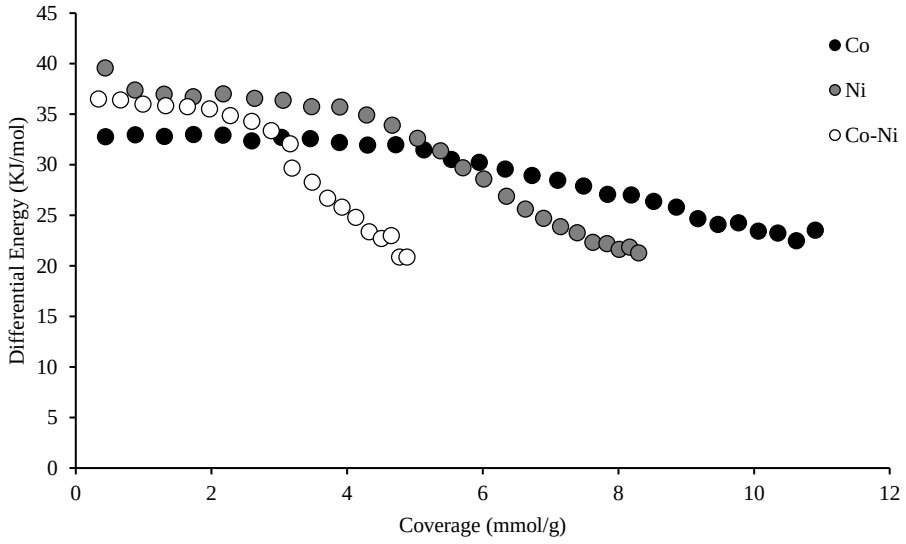

Figure 3-17: The differential adsorption energies of CO_2 on pure Co, Ni, and mixed-metal MOF-74

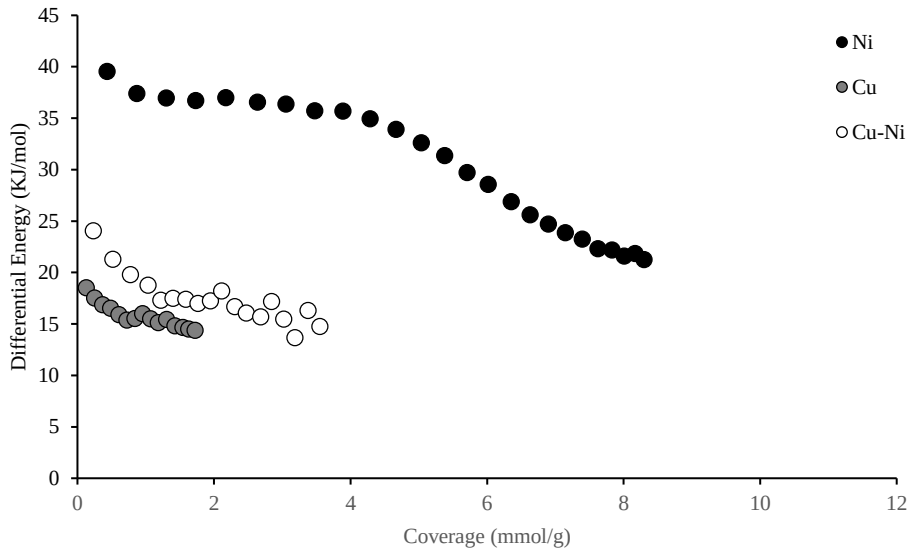

Figure 3-18: The differential adsorption energy of CO_2 on pure Ni, Cu and mixed-metal MOF-74

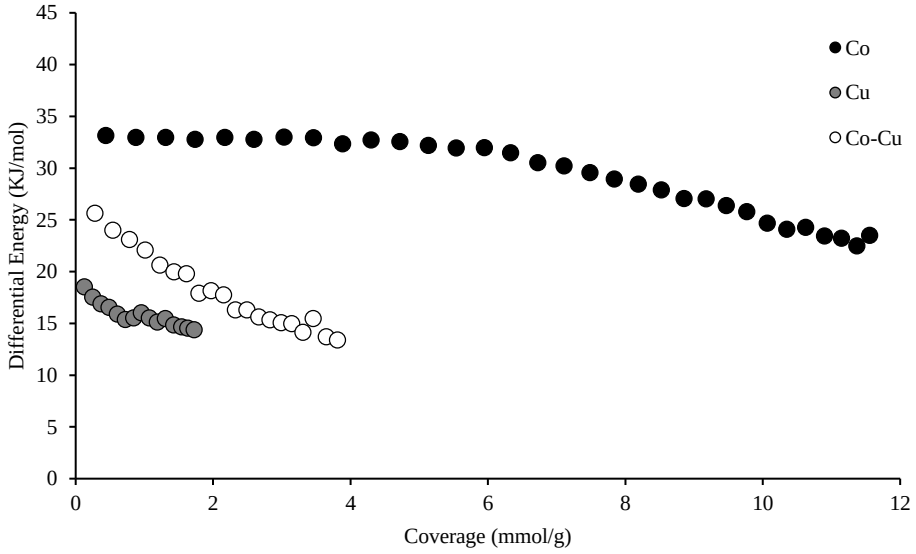

Figure 3-19: The differential adsorption energy of CO_2 on pure Co, Cu and mixed-metal MOF-74

In general, the order of differential heats is *methane* < *ethane* < *CO_2* < *ethylene* < *acetylene*. In order of pure metals, the order of differential heats is *Cu* < *Ni* < *Co* with the exception of acetylene, which showed a higher heat of adsorption for Ni compared to Co.

This is an interesting result, particularly because there is significant interest in using MOFs to separate acetylene and ethylene. While the heat of adsorption for Co-MOF-74 is essentially identical for ethylene and acetylene, the heat of adsorption for the Ni-MOF-74 was 15%-20% higher for acetylene compared to ethylene. In addition, there is a 38% difference between the theoretically predicted heat of adsorption for acetylene on Ni-MOF-74 and what was experimentally measured. This suggests that more work is needed to better understand and predict the adsorption behavior of acetylene on Ni-MOF-74.

3.5 Proposed Future Work

In regard to conducting fundamental studies of mixed-metal MOFs, it may be beneficial to consider other combinations of metals. For example, Co, Ni, and Cu have atomic numbers of 27, 28, and 29 and the corresponding lattice parameters in the MOF structures are similar. This makes it difficult to distinguish pure and mixed-metal MOFs by XRD. Another consideration for future work is growing single crystals large enough for SCXRD so that one can better understand the location of the different metals in a mixed-metal MOF structure. It is also suggested that low temperature calorimetry be performed on Ni-MOF-74, for ethylene and acetylene. This may provide additional insights into the differences in adsorption behavior between the adsorption of ethylene and acetylene on Ni-MOF-74. In addition, it would be valuable to collaborate with a computational group to better understand why such a difference is observed for Ni-MOF-74 but not Co-MOF-74, despite the currently computational modeling work in the

literature predicting similar adsorption behavior for both MOFs. Finally, another factor worth exploring is the adsorption behavior of unsaturated and saturated hydrocarbons. Lower than predicted heats of adsorption were experimentally measured with saturated adsorbates and higher than expected values with unsaturated adsorbates.

4. Conclusions

The initial goals of the UiO-66 project were to investigate the adsorption behavior of C_2 hydrocarbons on a multi-pore MOF. Through a combination of room and low temperature measurements, it was established that both confinement effects and electrostatic potential dominates binding energy of the adsorbate in the pore. UiO-66 with a bulkier group and polar adsorbate had higher adsorption energies, indicating a stronger interaction. Second, the low temperature measurements resolved the heat of adsorption for two types of binding sites for ethylene and ethane. However, the acetylene adsorption experiments suggest there is a third type of binding site that strongly interacts with acetylene. The nature of that adsorption site is currently under investigation.

The initial goals of the mixed-metal MOF-74 project was to investigate differences in the adsorption behavior of pure and mixed-metal MOF-74. For mixed-metal MOFs containing Cu, the heats of adsorption were similar to those of the pure Cu-MOF. For the Co-Ni mixed-metal MOF, the heat of adsorption was an average of the pure MOFs. Unexpectedly, the heat of adsorption of acetylene on Ni-MOF-74 was 15%-20% higher than ethylene, despite theoretical computations predicting similar heats of adsorption.

5. References

1. Vaughn, O. Porous by Design. *Nature News*, Nature Publishing Group, **17 July 2014**, www.nature.com/milestones/milecrystal/full/milecrystal22.html.

2. Wang, L.J.; Deng, H.; Furukawa, H.; Gándara, F.; Cordova, K.E.; Peri, D.; Yaghi, O.M. Synthesis and Characterization of Metal–Organic Framework-74 Containing 2, 4, 6, 8, and 10 Different Metals. *Inorganic Chemistry* **2014** *53* (12), 5881-5883

3. Greeves, N. ChemTube3D. *ChemTube3D*, University of Liverpool, www.chemtube3d.com/.

4. Burtch, N.C.; Jasuja, H.; Walton, K.S. Water Stability and Adsorption in Metal–Organic Frameworks. *Chemical Reviews*, **2014** *114* (20), 10575–10612.

5. Cavka, J. H.; Jakobsen, S.; Olsbye, U.; Guillou, N.; Lamberti, C.; Bordiga, S.; Lillerud, K. P. A New Zirconium Inorganic Building Brick Forming Metal Organic Frameworks with Exceptional Stability. *Journal of the American Chemical Society* **2008**, *130* (42), 13850–13851.

6. Biswas, S.; Voort, P. V. D. A General Strategy for the Synthesis of Functionalised UiO-66 Frameworks: Characterization, Stability and CO2 Adsorption Properties. *European Journal of Inorganic Chemistry* **2013**, *2013*(12), 2154–2160

7. Cmarik, G. E.; Kim, M.; Cohen, S. M.; Walton, K. S. Tuning the Adsorption Properties of UiO-66 Via Ligand Functionalization. *Langmuir* **2012**, *28* (44), 15606–15613.

8. Wu, H.; Chua, Y. S.; Krungleviciute, V.; Tyagi, M.; Chen, P.; Yildirim, T.; Zhou, W. Unusual and Highly Tunable Missing-Linker Defects in Zirconium Metal-Organic Framework UiO-66 and Their Important Effects on Gas Adsorption. *Journal of the American Chemical Society* **2013**, *135* (28), 10525–10532.

10. Wiersum, A. D.; Soubeyrand-Lenoir, E.; Yang, Q.; Moulin, B.; Guillerm, V.; Yahia, M. B.; Bourrelly, S.; Vimont, A.; Miller, S.; Vagner, C.; Daturi, M.; Clet, G.; Serre, C.; Maurin, G.; Llewellyn, P. L. An Evaluation of UiO-66 for Gas-Based Applications. *Chemistry - An Asian Journal* **2011**, *6* (12), 3270–3280.

11. Shearer, G. C.; Chavan, S.; Ethiraj, J.; Vitillo, J. G.; Svelle, S.; Olsbye, U.; Lamberti, C.; Bordiga, S.; Lillerud, K. P. Tuned to Perfection: Ironing Out the Defects in Metal-Organic Framework UiO-66. *Chemistry of Materials*, **2014**, *26* (14), 4068-4071.

12. Miguel, G.I.; Kapelewski, M.T.; Bloch, E. D.; Milner, P.J.; Reed, D.A.; Hudson, M.R.; Mason, J.A.; Barin, G.; Brown, C.M.; Long, J.R. Separation of Xylene Isomers through Multiple Metal Site Interactions in Metal–Organic Frameworks. *Journal of the American Chemical Society* **2018** *140* (9), 3412-3422

13. Nijem, N.; Wu, H.; Canepa, P.; Marti, A.; Balkus, K. J.; Thonhauser, T.; Li, J.; Chabal, Y. J. Tuning the Gate Opening Pressure of Metal Organic Frameworks

(MOFs) for the Selective Separation of Hydrocarbons. *Journal of the American Chemical Society* **2012**, *134* (37), 15201–15204.

14. Myers, A. L. Thermodynamics of Adsorption in Porous Materials. *AIChE Journal* **2002**, *48* (1), 145–160.

15. Alezi, D.; Belmabkhout, Y.; Suyetin, M.; Bhatt, P. M.; Weseliński, Ł. J.; Solovyeva, V.; Adil, K.; Spanopoulos, I.; Trikalitis, P. N.; Emwas, A.-H.; Eddaoudi, M. MOF Crystal Chemistry Paving the Way to Gas Storage Needs: Aluminum-Based Soc-MOF for CH4, O2, and CO2 Storage. *Journal of the American Chemical Society* **2015**, *137* (41), 13308–13318.

16. Glover, T. G.; Peterson, G. W.; Schindler, B. J.; Britt, D.; Yaghi, O. MOF-74 Building Unit Has a Direct Impact on Toxic Gas Adsorption. *Chemical Engineering Science* **2011**, *66* (2), 163–170.

17. Morris, R. E.; Wheatley, P. S. ChemInform Abstract: Gas Storage in Nanoporous Materials. *ChemInform* **2008**, *39* (35).

18. Li, H.; Wang, K.; Sun, Y.; Lollar, C. T.; Li, J.; Zhou, H.-C. Recent Advances in Gas Storage and Separation Using Metal–Organic Frameworks. *Materials Today* **2018**, *21* (2), 108–121.

19. Tan, K.; Zuluaga, S.; Gong, Q.; Gao, Y.; Nijem, N.; Li, J.; Thonhauser, T.; Chabal, Y. J. Competitive Coadsorption of CO2 with H2O, NH3, SO2, NO, NO2, N2, O2, and CH4 in M-MOF-74 (M = Mg, Co, Ni): The Role of Hydrogen Bonding. *Chemistry of Materials* **2015**, *27* (6), 2203–2217.

20. Lewandowski, S. Big Changes Ahead for Ethylene Implications for Asia. *IHS Markit Conference,* Singapore **2016**

21. Hu, T.-L.; Wang, H.; Li, B.; Krishna, R.; Wu, H.; Zhou, W.; Zhao, Y.; Han, Y.; Wang, X.; Zhu, W.; Yao, Z.; Xiang, S.; Chen, B. Microporous Metal–Organic Framework with Dual Functionalities for Highly Efficient Removal of Acetylene from Ethylene/Acetylene Mixtures. *Nature Communications* **2015**, *6* (1).

22. Eldridge, R.B. Olefin/parrafin separation technology: a review. *Industrial Engineering and Chemical Research*, **1993**, *32*, 2208-2212.

23. Ren, T.; Patel, M.; Blok, K. Olefins from Conventional and Heavy Feedstocks: Energy Use in Steam Cracking and Alternative Processes. *Fuel and Energy Abstracts* **2006**, *47* (4), 425–451.

24. Mofarahi, M.; Salehi, S. M. Pure and Binary Adsorption Isotherms of Ethylene and Ethane on Zeolite 5A." *Adsorption* **2012**, *19* (1), 101–110.

25. Katz, M. J.; Brown, Z. J.; Colón, Y. J.; Siu, P. W.; Scheidt, K. A.; Snurr, R. Q.; Hupp, J. T.; Farha, O. K. A Facile Synthesis of UiO-66, UiO-67 and Their Derivatives." *Chemical Communications* **2013**, *49* (82), 9449.

26. Yang, Q.; Wiersum, A. D.; Llewellyn, P. L.; Guillerm, V.; Serre, C.; Maurin, G. Functionalizing Porous Zirconium Terephthalate UiO-66(Zr) for Natural Gas Upgrading: A Computational Exploration. *Chemical Communications* **2011,** 47 (34) 9603

27. Granadeiro, C. M.; Ribeiro, S. O.; Karmaoui, M.; Valença, R.; Ribeiro, J. C.; Castro, B. D.; Cunha-Silva, L.; Balula, S. S. Production of Ultra-Deep Sulfur-Free Diesels Using a Sustainable Catalytic System Based on UiO-66(Zr). *Chemical Communications* **2015**, *51* (72), 13818–13821.

28. Burtch, N. C.; Walton, K. S. Modulating Adsorption and Stability Properties in Pillared Metal–Organic Frameworks: A Model System for Understanding Ligand Effects. *Accounts of Chemical Research* **2015**, *48* (11), 2850–2857.

29. Liu, H.; Zhao, Y.; Zhang, Z.; Nijem, N.; Chabal, Y. J.; Zeng, H.; Li, J. The Effect of Methyl Functionalization on Microporous Metal-Organic Frameworks' Capacity and Binding Energy for Carbon Dioxide Adsorption. *Advanced Functional Materials* **2011**, *21* (24), 4754–4762.

30. Myers, A. L. Thermodynamics of Adsorption in Porous Materials. *AIChE Journal*, **2005** *48* (1), 145–160.

31. Builes, S.; Sandler, S. I.; Xiong, R. Isosteric Heats of Gas and Liquid Adsorption. *Langmuir* **2013**, *29* (33), 10416–10422.

32. Parrillo, D.; Gorte, R. Design Parameters for the Construction and Operation of Heat-Flow Calorimeters. *Thermochimica Acta* **1998**, *312* (1-2), 125–132.

33. Shen, D.; Bulow, M.; Siperstein, F.; Engelhard, M.; Myers, A.L. Comparison of experimental techniques for measuring isosteric heat of adsorption. *Adsorption* **2000** *6* (4), 275-286.

34. Rouquerol Françoise; Rouquerol, J.; Sing, K. S. W.; Llewellyn, P. L.; Maurin, G. *Adsorption by Powders and Porous Solids: Principles, Methodology and Applications*; Elsevier/AP: Amsterdam, 2014.

35. Thommes, M.; Kaneko, K.; Neimark, A. V.; Olivier , J. P.; Rodriguez-Reinoso, F.; Rouquerol, J.; Sing , K. S. W. Physisorption of Gases, With Special Reference to the Evaluation of Surface Area and Pore Size Distribution (IUPAC Technical Report). *IUPAC Standards Online* **2016**, *33* (2).

36. Biswas, S.; Voort, P. V. D. A General Strategy for the Synthesis of Functionalised UiO-66 Frameworks: Characterisation, Stability and CO2 Adsorption Properties. *European Journal of Inorganic Chemistry* **2013**, *2013* (12), 2154–2160.

37. Wiersum, A. D.; Soubeyrand-Lenoir, E.; Yang, Q.; Moulin, B.; Guillerm, V.; Yahia, M. B.; Bourrelly, S.; Vimont, A.; Miller, S.; Vagner, C.; Daturi, M.; Clet, G.; Serre, C.; Maurin, G.; Llewellyn, P. L. An Evaluation of UiO-66 for Gas-Based Applications. *Chemistry – An Asian Journal*, **2011,** 6, 3270-3280.

38. Lipkowitz, K.B. and Boyd, D.B., *Calculation and display of the electric potential* From *Reviews in Computational Chemistry II*, Wiley-VCH, Inc. **1991**, 226-232.

39. Nicholson, T. M.; Bhatia, S. K. Electrostatically Mediated Specific Adsorption of Small Molecules in Metallo-Organic Frameworks. *The Journal of Physical Chemistry B* **2006**, *110* (49), 24834–24836.

40. Shearer, G. C.; Chavan, S.; Bordiga, S.; Svelle, S.; Olsbye, U.; Lillerud, K. P. Defect Engineering: Tuning the Porosity and Composition of the Metal–

Organic Framework UiO-66 via Modulated Synthesis. *Chemistry of Materials* **2016**, *28* (11), 3749–3761.

41. Trickett, C. A.; Gagnon, K. J.; Lee, S.; Gándara, F.; Bürgi, H.-B.; Yaghi, O. M. Definitive Molecular Level Characterization of Defects in UiO-66 Crystals. *Angewandte Chemie* **2015**, *127* (38), 11314–11319.

42. Caratelli, C.; Hajek, J.; Cirujano, F. G.; Waroquier, M.; Xamena, F. X. L. I.; Speybroeck, V. V. Nature of Active Sites on UiO-66 and Beneficial Influence of Water in the Catalysis of Fischer Esterification. *Journal of Catalysis* **2017**, *352*, 401–414.

43. Hu, T.-L.; Wang, H.; Li, B.; Krishna, R.; Wu, H.; Zhou, W.; Zhao, Y.; Han, Y.; Wang, X.; Zhu, W.; Yao, Z.; Xiang, S.; Chen, B. Microporous Metal–Organic Framework with Dual Functionalities for Highly Efficient Removal of Acetylene from Ethylene/Acetylene Mixtures. *Nature Communications* **2015**, *6* (1).

44. Moreau, F.; Silva, I. D.; Smail, N. H. A.; Easun, T. L.; Savage, M.; Godfrey, H. G. W.; Parker, S. F.; Manuel, P.; Yang, S.; Schröder, M. Unravelling Exceptional Acetylene and Carbon Dioxide Adsorption within a Tetra-Amide Functionalized Metal-Organic Framework. *Nature Communications* **2017**, *8*, 14085.

45. Yarris, L. An Inside Look at a MOF in Action. https://newscenter.lbl.gov/2013/11/22/an-inside-look-at-a-mof-in-action/ **2013**

46. Gonzalez, M. I.; Kapelewski, M. T.; Bloch, E. D.; Milner, P. J.; Reed, D. A.; Hudson, M. R.; Mason, J. A.; Barin, G.; Brown, C. M.; Long, J. R. Separation of Xylene Isomers through Multiple Metal Site Interactions in Metal–Organic

Frameworks. *Journal of the American Chemical Society* **2018**, *140* (9), 3412–3422.

47. Campbell, J.; Tokay, B. Controlling the Size and Shape of Mg-MOF-74 Crystals to Optimise Film Synthesis on Alumina Substrates. *Microporous and Mesoporous Materials* **2017**, *251*, 190–199.

48. Lee, K.; Howe, J. D.; Lin, L.-C.; Smit, B.; Neaton, J. B. Small-Molecule Adsorption in Open-Site Metal–Organic Frameworks: A Systematic Density Functional Theory Study for Rational Design." *Chemistry of Materials* **2015**, *27* (3), 668–678.

49. Lee S.; Bürgi, H.B.; Alshmimri, S.A.; Yaghi, O.M. Impact of Disordered Guest–Framework Interactions on the Crystallography of Metal–Organic Frameworks. *Journal of the American Chemical Society* **2018** *140* (28), 8958-8964

50. Wong-Ng, W.; Kaduk, J. A.; Wu, H.; Suchomel, M. Synchrotron X-ray studies of metal-organic framework M_2(2,5-dihydroxyterephthalate), *M* = (Mn, Co, Ni, Zn) (MOF74). *Powder Diffraction* **2012**, *27* (4), 256–262.

Appendix

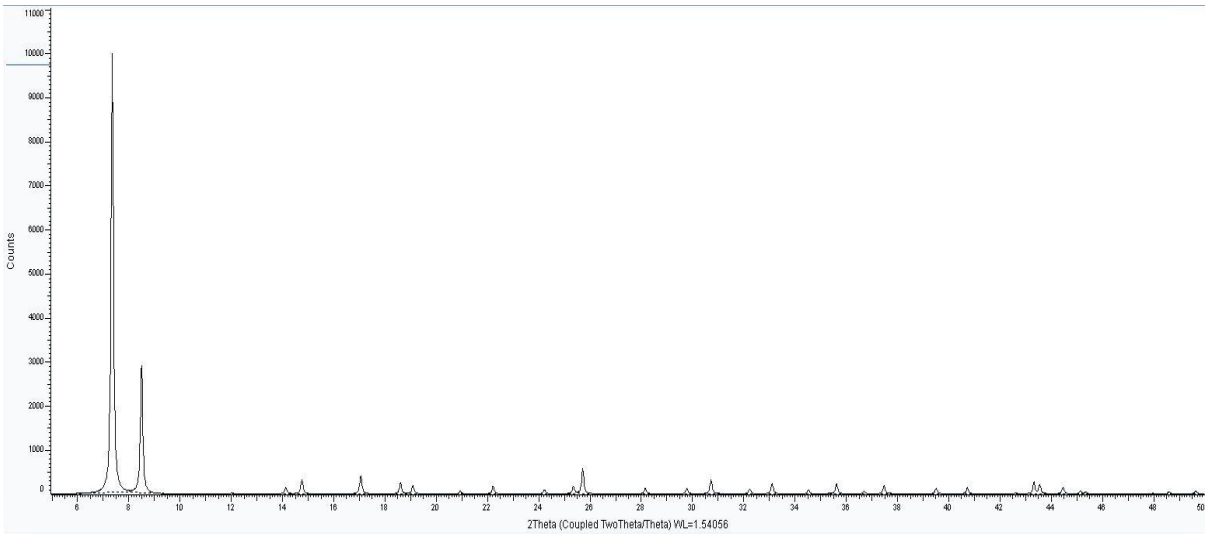

A 1: A reference PXRD scan for UiO-66, collected on a Synchrotron XRD machine by the University of Berkeley

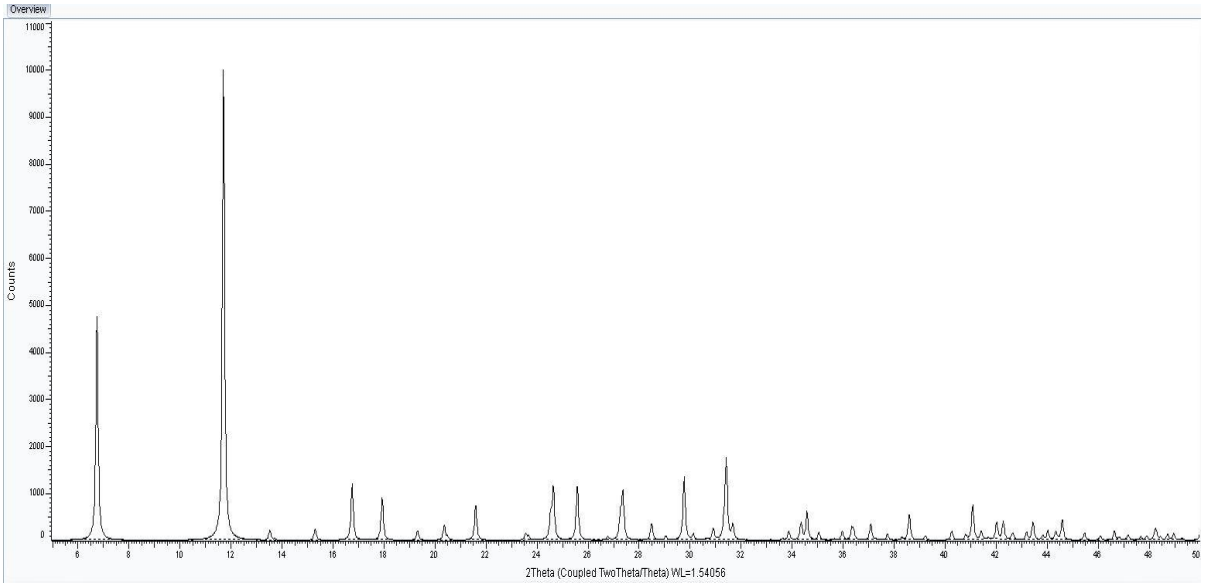

A 2: A reference PXRD scan for Co-MOF-74, collected on a Synchroton XRD machine by the International Centre for Diffraction Data.[50]

Curriculum Vitae

Taylor Ellise Barrett

Born: June 16th
Augusta, Georgia

Undergraduate Study: Wake Forest University
Winston Salem, NC 27109
BA Chemistry, minor in Biology, 2017

Graduate Study: Wake Forest University
Winston Salem, NC 27109
MS Chemistry, 2019 (anticipated)
Advisor: Dr. Michael D. Gross
Thesis title: A Calorimetric Study of Light Hydrocarbon Adsorption on Metal-Organic Frameworks

Experience:

Graduate Research Assistant at Wake Forest University	2017-2019
Undergraduate Research Student at Wake Forest University	2016-2017
Resident Adviser at Wake Forest University	2014-2017

Publications:

Muhoza, S. P., Barrett, T. E., Cottam, M. A., Soll, S. E., Yuce, M. D., Prathab, V. S., . . . Gross, M. D. (2018). High Surface Area SOFC Electrode Materials Prepared at Traditional Sintering Temperatures. *Journal of The Electrochemical Society, 165*(2). doi:10.1149/2.0381802jes

Muhoza, S. P., Barrett, T. E., Soll, S. E., & Gross, M. D. (2017). Nanostructured SOFC Electrode Scaffolds Prepared via High Temperature in-situ Carbon Templating of Hybrid Materials. *ECS Transactions, 78*(1), 1407-1416. doi:10.1149/07801.1407ecst

Presentations:

Barrett, T.E.; Gross, M.D.; Calorimetric adsorption study of light hydrocarbons on functionalized UiO-66 MOF. *Spring 2019 National ACS meeting; Orlando, Fl, March 31st-April 4th, 2019*

Barrett, T.E.; Gross, M.D.; Calorimetric adsorption study of light hydrocarbons on functionalized UiO-66 MOF. *70th SERMACS regional meeting; Augusta, GA, October 31st-November 3rd, 2018*

Awards:

Alumni Student Travel Award	2019
WFU Center for Energy and Sustainability Environmental Fellow	2016
RLH Event Coordinator of the Year	2016, 2017